Intelligent Covert Satellite Communication for Military Robot Swarm

CHAOFAN CHEN[1], **SHUAI WANG**[1], (Member, IEEE), **LI LI**[2], **SHENG KE**[1],
CHANGHONG WANG[1], **AND XIANGYUAN BU**[1]

[1]School of Information and Electronics, Beijing Institute of Technology, Beijing 100081, China
[2]Provincial Key Laboratory of Information Coding and Transmission, Southwest Jiaotong University, Chengdu 610031, China

Corresponding author: Shuai Wang (swang@bit.edu.cn)

ABSTRACT Military robot swarm becomes more and more important for contemporary military application. In order to satisfy sophisticated application scenarios, novel communication architecture for military robot swarm has to be conceived. In this paper, we propose a multi-carrier intelligent covert satellite communication (MCICSC) architecture based on electromagnetic environment sensing technology, in where the ability of dynamically adapting the system configuration to the holistic requirements of covertness, performance, and complexity can be considerably improved. Additionally, in order to solve the carrier synchronization problem in very low signal noise ratio (SNR) for each data stream of MCICSC, polar code (PC) is incorporated into the proposed MCICSC system. With the aid of the proposed polar code-aided multi-stream parallel feedback (PAMSPF) carrier synchronization scheme, the MCICSC system is capable of realizing high-precise carrier synchronization even in very low SNR region. Moreover, in order to further decrease the complexity of our MCICSC system, we also propose a polar code-based diversity combining (PBDC) scheme, which is capable of efficiently combing all the data streams without the aid of channel state information (CSI) estimation. Numerical simulations demonstrate that for MCICSC system the performance of the PAMSPF carrier synchronization and PBDC combining schemes can get extremely close to that of an ideally synchronized system. Complexity analysis of the proposed algorithms is given as well.

INDEX TERMS Robot swarm, satellite communication, multi-carrier synchronization, polar codes, covert communication, iterative decoding.

I. INTRODUCTION

Robot swarm has attracted lots of attentions in the past decades and has achieved rapid development with the aid of Artificial Intelligence [1], [2]. Generally, a robot swarm consisting of hundreds and thousands of small robots can support some complex tasks based on the collaborations among its robot members. Additionally, due to its characteristics of intelligence, maneuverability, flexibility and high survivability, the robot swarm has been applied to various military scenarios [3], [4]. Typical applications include front operations, emergency management, intelligence collection and enemy reconnaissance. For example, cooperated with unmanned aerial vehicle (UAV)-assisted networking system [5]–[7], the robot swarm can be deployed at some sensitive areas,

The associate editor coordinating the review of this manuscript and approving it for publication was Jiankang Zhang.

such as government classified regions, military combat zones and costal border waters, for intelligently gathering information. Commonly, the information collected by the robot swarm is confidential and time-limited, so the information should be transmitted back to the remote information center in a fast and secure way. In particular, in order to preventing the back-forward information from being detected and intercepted by hostile forces, the covert transmission is required.

In order to support long distance transmission, satellite communication becomes an efficient solution [8]–[11]. The satellite communication can support secure and low latency data transmission and overcome various limitations of geographic conditions, operation environment and transmission distance. Hence it demonstrates lots of inherent advantages in support of the remote information transmission of military robot swarms [12]. Furthermore, considering the covert transmission demands in complex situations, the intelligent covert

satellite communication is an appropriate choice for military robot swarms. Therefore, the uplink of the intelligent covert satellite communications, where the data is transmitted from the robot swarm to the satellite becomes the main research scope in this paper.

Additionally, polar codes (PCs), since proposed by Arıkan [13], have been applied to a variety of areas, such as magnetic recording [14], internet of things (IoT) [15], [16], light communications [17], and the fifth generation (5G) communications [18]–[20], because, it has a low computational complexity and a near-capacity performance. Furthermore, except for the application in coherent detection systems, polar codes are also applied to noncoherent detection systems [21], [22]. In addition, after its original successive cancellation (SC) decoding algorithm, various more advanced decoding algorithms, such as successive cancellation list (SCL) [23], successive cancellation stack (SCS) [24], belief propagation (BP) [25] and the-state-of-the-art ones [26]–[28], have been consecutively proposed.

It is well-known that the PCs outperform the low density parity check codes (LDPC) in small packet transmission [23], [29]. In covert satellite communication, the data is normally transmitted in form of short burst frames for guaranteeing the covertness. Hence, it motive us to invoke polar code into covert satellite communication system. In [30], based on binary polar codes a covert communication code for binary-input asynchronous discrete memoryless channels was proposed. However in covert satellite communication, the data is normally transmitted over a synchronous discrete memoryless channel. Thus, the method in [30] is not suitable for covert satellite communication systems. Hence, to the best of our knowledge, how to efficiently invoke polar codes into the covert satellite communication systems is still an open problem.

The traditional ways to realize the communication covertness can be categorized into two classes: physical layer-related methods and application layer-related methods. The former commonly relies on the short frame transmission, spread spectrum technology and multiple beam forming technology. The latter usually relies on the applications of encryption algorithms [31], [32]. However, neither relying on the former class nor the latter class can afford further complexity increase. Hence, a more efficient covert satellite communication scheme has to be developed for supporting the new requirement of contemporary battlefield.

Against the background, in this paper we firstly construct a new covert satellite communication system, which is motivated by multicarrier direct sequence code-division multiple access (MC-DS-CDMA) systems [33]. More specifically, for the uplink communication of the proposed system, before the transmission process, we sense the environmental electromagnetic signals first. Then, we transmit our information carrying signal in the same band as that of the sensed signals. By this way, we equivalently hide the useful data under the environment electromagnetic signals. Furthermore, polar codes are specifically designed for the proposed scheme

and play a critical role in the information protection, carrier synchronization as well as information diversity combing.

The contributions of this paper can be summarized as follow:

1) We propose a novel intelligent covert satellite communication architecture, in which the involved parameters could be flexibly configured for adapting to various practical scenarios.

2) A polar code-aided multi-stream parallel feedback (PAMSPF) carrier synchronization algorithm is designed to achieve a high-precision and low-complexity carrier synchronization, which paves the solid way for the sequential processes of data stream diversity combination and final information recovery.

3) A polar code-based diversity combing (PBDC) algorithm is proposed. Without the channel state information (CSI), the proposed combing algorithm can achieve considerably low complexity at the cost of a very slight performance loss compared to the optimal maximum ratio combining (MRC) method.

The remainder of this paper is organized as follows: In Section II, some fundamental techniques are introduced, including MC-DS-CDMA scheme, polar codes and expectation maximization (EM) algorithm. The proposed intelligent covert satellite communication models and corresponding synchronization and combining algorithms are presented in Section III. Abundant of numerical simulation results and corresponding discussions are provided in Section IV. Associated complexity of the proposed algorithms is analysed in Section V. Finally, we conclude in Section VI.

In this paper, the following notation rules are obeyed except for special instructions. We would use a lower case bold letter, such as $\mathbf{x}$, to denote a row vector and a lower case letter with a subscript, such as x_i, as its corresponding ith element. We use $x_i^j = (x_i, x_{i+1}, \dots, x_j)$ to denote a sub-vector of vector $\mathbf{x}$, which starts from the ith element and terminated at the jth element. We use an upper case bold letter to represent a matrix and an upper case letter with a pair of subscripts to represent its element, for example, X_{ij} denotes the element of matrix $\mathbf{X}$ in ith row and jth column. Symbol $(\cdot)^T$ represents the transpose of a vector or a matrix. Symbol $(\cdot)^*$ calculates the conjugacy. In addition, notations $\bigotimes$ and $\|\cdot\|$ denote the Kronecker product and the cardinality, respectively.

II. PRELIMINARY

A. MULTICARRIER DIRECT SEQUENCE CODE-DIVISION MULTIPLE ACCESS

As described in [34], MC-DS-CDMA scheme is originally proposed by introducing orthogonal frequency-division multiplexing (OFDM) to DS-CDMA scheme. Single carrier DS-CDMA (SC-DS-CDMA) scheme only use one carrier to transmit signals. In contrast, in MC-DS-CDMA scheme, signals are modulated to multiple subcarriers. It employs both time domain (T-domain) and frequency domain (F-domain) spreading and hence is called as TF-domain spreading type
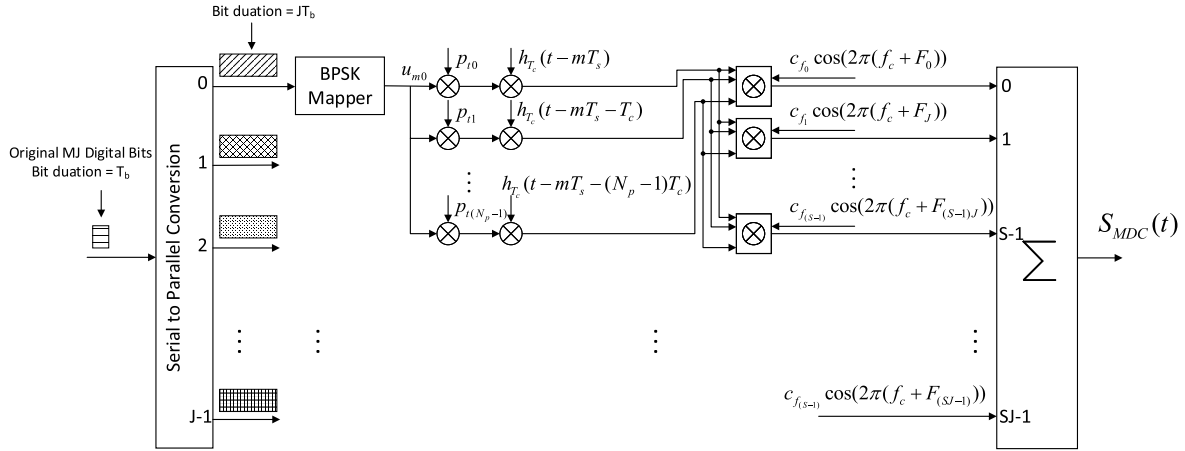
FIGURE 1. Transmitter architecture of MC-DS-CDMA scheme.

of MC-DS-CDMA [35]. Herein, we focus on its transmitter structure, which is shown in Fig. 1. Inspired by its structure, we propose a novel intelligent covert satellite communication structure in later section(see Section III-A).

As seen in Fig. 1, original data stream is firstly transferred into multiple rate-reduced parallel streams with the aid of serial to parallel conversion. On each stream, data bits are successively mapped according to binary phase shift keying (BPSK). Then, the data stream is spread by the corresponding specific N_p-chip pseudo-noise (PN) code, $\{p_1, p_2, \ldots, p_{N_p}\}$, and then reshaped by specific waveform. In the last step, it is modulated to its corresponding subcarrier. Finally, All signals from each data stream are combined into one. Accordingly, the transmitted MC-DS-CDMA signal can be formulated as

$$S_{MDC}(t) = \sqrt{\frac{2P}{JS}} \sum_{m=0}^{M-1} \sum_{j=0}^{J-1} \sum_{s=0}^{S-1} \sum_{k=0}^{N_p-1} u_{mj}$$
$$\times p_{tk} h_{T_c}(t - mT_s - kT_c) c_{fs} \cos(2\pi(f_c + F_{sJ+j})t), \tag{1}$$

where P denotes the transmit power, J is the number of bits carried by a MC-DS-CDMA symbol. S represents the number of subcarriers used for F-domain spreading, and M is the number of MC-DS-CDMA symbols conveyed in once burst transmission through all the parallel branches. $u_{mj} \in \{+1, -1\}$ denotes the BPSK symbol, which relates to the jth bit carried by the mth MS-DS-CDMA symbol. The duration of a MS-DS-CDMA symbol is JT_b. Furthermore, p_{tk} and c_{fs} are respectively the kth chip of the T-domain spreading code and s^{th} chip of the F-domain spreading code. T_s and T_c represent symbol and chip duration, respectively. $h_\tau(t)$ is the chip waveform employed in the interval of $[0, \tau]$. In addition, $\{f_c + F_{sJ+j}\}$ represents the central subcarrier frequency employed by the sth F-domain chip of the jth bit. It implies that a total number of SJ central subcarrier frequencies are required by MC-DS-CDMA systems. In particular, all the J parallel data streams use the same T-domain spreading code, which is represented by $p_{tk}|_{k=0}^{k=N_p-1}$ in (1). Frequency offset

between any two adjacent subcarriers are the same in the MC-DS-CDMA systems.

By simultaneously executing the T-domain and F-domain (namely, TF-domain) spreading, MC-DS-CDMA systems can achieve the processing gain that equals the product of the T-domain and F-domain spreading factors, which is beneficial for increasing the user capacity.

B. POLAR CODES
Polar codes are based on the phenomenon of "channel polarization", *i.e*, with the aid of the recursive channel splitting and combining, the split channels will tend to be either completely noisy or absolutely error-free. Furthermore, as the code length increases, the fraction of error-free channels will tend to the channel symmetric capacity of the experienced binary input discrete memoryless channel (B-DMC) [13]. Thus, the information bits will be placed at the relatively noiseless channels. In contrast, the frozen bits, which are usually constant zeros and known to receiver will be transmitted through the other channels.

In essential, polar codes belong to the linear block codes (LBC). Hence, it can be simply specified by its generation matrix $\mathbf{G}$. In more detail, for any integer $n \in \mathbb{N}$, let $N = 2^n$ be the code length and $K < N$ be the information bit length. Let $\mathcal{A}$ and $\mathcal{A}^C$ denote the index sets of *information bits* and *frozen bits*, respectively. They satisfy $\|\mathcal{A}\| = K$ and $\|\mathcal{A}^C\| = N - K$. Furthermore, the two sets also hold the relation of $\mathcal{A} \cup \mathcal{A}^C = \{1, 2, \ldots, N\}$. Then, let $\mathbf{u} = \mathbf{u}_\mathcal{A} \cup \mathbf{u}_{\mathcal{A}^C}$ be the bit sequence input in the polar encoder, where $\mathbf{u}_\mathcal{A}$ corresponds to *information bits* and $\mathbf{u}_{\mathcal{A}^C}$ *frozen bits*. Let $\mathbf{B_N}$ be a bit-reverse permutation matrix which has the function of reversing n bits binary representation of a integer from $b_n, b_{n-1}, \ldots, b_1$ to $b_1, b_2, \ldots, b_n$. Then, let $\mathbf{F}^{\otimes \mathbf{n}} = \mathbf{F} \otimes \mathbf{F}^{\otimes \mathbf{n}-1}$ be the nth order Kronecker power of the kernel matrix $\mathbf{F} = \begin{pmatrix} 1 & 0 \\ 1 & 1 \end{pmatrix}$. According to above definitions, the polar encoding process can be denoted as

$$\mathbf{x} = \mathbf{uG} = (\mathbf{u}_\mathcal{A} + \mathbf{u}_{\mathcal{A}^C})\mathbf{B_N}\mathbf{F}^{\otimes \mathbf{n}}, \tag{2}$$

where $\mathbf{x} = x_1^N = (x_1, x_2, \ldots, x_N)$ is the encoded polar codeword.

There are two major kinds of decoding algorithms: successive cancellation (SC)-based kind and belief propagation (BP)-based kind. The SC-based algorithms perform serial decoding process and they belong to hard-decision algorithms. In contrast, the BP-based algorithms execute fully parallel decoding process and are capable of providing soft likelihood values. In more depth, according to the type of matrix employed for generating the BP decoding factor graph, BP-based polar decoding algorithms can be further classified into generation matrix based BP (G-based BP) and parity check matrix based BP (H-based BP). For more details of these decoding algorithms, we would like to refer to literatures of [25], [36]–[38].

C. EXPECTATION MAXIMIZATION ALGORITHM

Expectation maximization (EM) algorithm was proposed in [39]. It has been broadly applied and proved to be an efficient method to iteratively complete the maximum likelihood (ML) estimation. In this iterative operations, the observations can be considered as incomplete data [40], [41]. In the ensuing interpretations, we would elaborate the principle of EM involved in synchronization applications.

Let us consider its signal processing model. The information sequence of $\mathbf{u} = (u_1, u_2, \ldots, u_L)$ is encoded to a codeword of $\mathbf{x} = (x_1, x_2, \ldots, x_N)$. Then, $\mathbf{x}$ is modulated to a sequence of symbols, namely $\mathbf{s} = (s_1, s_2, \ldots, s_D)$. All of its elements s_d belong to the same alphabet $\mathcal{S}$, whose cardinality is $\mathcal{M}$. Herein, we focus on the bandpass transmission over an additive white Gaussian noise (AWGN) channel. Accordingly, the received signal is given by

$$r(t) = A \sum_{k=1}^{D} s_k g(t - kT_s - \tau) \exp(j(2\pi \Delta ft + \theta)) + n(t), \quad (3)$$

where T_s is the symbol period and $g(t)$ is a shaping pulse function. $n(t)$ denotes an AWGN noise having a zero mean and a variance of N_0. In addition, A, τ, Δf and θ are synchronization parameters that we want to estimate. They are the channel amplitude, signal delay, carrier frequency offset and phase offset, respectively. For simplicity, we define a new parameter $\mathbf{b}$ composed by all the above parameters, which is written as $\mathbf{b} \triangleq \langle A, \tau, \Delta f, \theta \rangle$.

According to the above addressed model and to the ML estimation rule, the ML estimation of $\mathbf{b}$ is given by

$$\hat{\mathbf{b}} = \arg\max_{\check{\mathbf{b}}} \log \Pr\{\mathbf{r}|\check{\mathbf{b}}\}. \quad (4)$$

According to the EM algorithm, two steps, namely, the expectation step (E-step) and the maximization step (M-step), will be implemented for solving (4). According to [42], these two steps can be formulated as

$$\text{E-step:} \mathcal{Q}\left(\mathbf{b}, \hat{\mathbf{b}}^{(l)}\right) = \int \Pr\{\mathbf{z}|\mathbf{r}, \hat{\mathbf{b}}^{(l)}\} \ln\left(\Pr\{\mathbf{z}|\mathbf{b}\}\right) d\mathbf{z}, \quad (5)$$

$$\text{M-step:} \hat{\mathbf{b}}^{(l+1)} = \arg\max_{\mathbf{b}} \mathcal{Q}\left(\mathbf{b}, \hat{\mathbf{b}}^{(l)}\right), \quad (6)$$

where superscript l denotes the iteration index and $\hat{\mathbf{b}}^{(l)}$ represents the estimate of $\mathbf{b}$ during the lth iteration. The actual observation set $\mathbf{r}$ and the extended observation set $\mathbf{z}$ are called as *incomplete* and *complete* data set, respectively. After establishing the system model of eq. (3) and formulating the two EM steps of eq. (5) $\sim$ (6), we will derive how to obtain the ML estimation of the frequency and phase offsets according to the EM algorithm. We focus on the estimation of phase and frequency offset. Hence, we assume that the channel amplitude and delay are already known at the receiver. Consequently, $\mathbf{b}$ is simplified to $\mathbf{b} = \langle \Delta f, \theta \rangle$. In particular, at time k, let us define $\phi_k = 2\pi k \Delta fT_s + \theta$. Thus, the sampled signal from the output of the matched filter can be formulated as

$$\begin{aligned} r_k &= s_k \exp(j\phi_k) + n_k \\ &= s_k \exp(j2\pi k \Delta fT_s + \theta) + n_k. \end{aligned} \quad (7)$$

Since we consider AWGN channels, the conditional probability of r_k can be written as

$$\Pr\{r_k|s_k, \phi_k\} = \frac{1}{\sqrt{2\pi}\sigma} \exp\left(-\frac{1}{2\sigma^2} \|r_k - s_k \exp(j\phi_k)\|^2\right). \quad (8)$$

Since $r_k, k = 1, 2, \ldots, D$ are independent random variables, then we can arrive at

$$\begin{aligned} &\Pr\{\mathbf{r}|\mathbf{s}, \phi\} \\ &= \prod_{k=1}^{D} \Pr\{r_k|s_k, \phi_k\} \\ &= \prod_{k=1}^{D} \left\{\frac{1}{\sqrt{2\pi}\sigma} \exp\left(-\frac{1}{2\sigma^2} \|r_k - s_k \exp(j\phi_k)\|^2\right)\right\} \\ &= \prod_{k=1}^{D} \left\{\frac{1}{\sqrt{2\pi}\sigma} \exp\left(-\frac{1}{2\sigma^2}\left(\|r_k\|^2 + \|s_k\|^2 \right.\right.\right. \\ &\qquad\qquad \left.\left.\left.- 2\Re\{r_k s_k^* \exp(-j\phi_k)\}\right)\right)\right\}. \end{aligned} \quad (9)$$

By neglecting the terms irrelevant to $\mathbf{s}$ and ϕ, (9) can be rewritten as

$$\begin{aligned} &\Pr\{\mathbf{r}|\mathbf{s}, \phi\} \\ &= \prod_{k=1}^{D} \left\{\frac{1}{\sqrt{2\pi}\sigma} \exp\left(-\frac{1}{2\sigma^2}\left(\|s_k\|^2 - 2\Re\{r_k s_k^* \exp(-j\phi_k)\}\right)\right)\right\}. \end{aligned} \quad (10)$$

Then, let us define the complete data set as $\mathbf{z} \triangleq [\mathbf{r}, \mathbf{s}]$ and substituting it to eq. (5), we could have

$$\begin{aligned} \mathcal{Q}\left(\mathbf{b}, \hat{\mathbf{b}}^{(l)}\right) &= \int \Pr\{\mathbf{z}|\mathbf{r}, \hat{\mathbf{b}}^{(l)}\} \ln\left(\Pr\{\mathbf{z}|\mathbf{b}\}\right) d\mathbf{z} \\ &= \int_{\mathbf{s}} \Pr\{\mathbf{s}|\mathbf{r}, \hat{\mathbf{b}}^{(l)}\} \ln\left(\Pr\{\mathbf{r}|\mathbf{s}, \mathbf{b}\} \Pr\{\mathbf{s}\}\right) d\mathbf{s} \\ &= \int_{\mathbf{s}} \Pr\{\mathbf{s}|\mathbf{r}, \hat{\mathbf{b}}^{(l)}\} \ln\left(\Pr\{\mathbf{r}|\mathbf{s}, \mathbf{b}\}\right) d\mathbf{s} \\ &\quad + \int_{\mathbf{s}} \Pr\{\mathbf{s}|\mathbf{r}, \hat{\mathbf{b}}^{(l)}\} \ln\left(\Pr\{\mathbf{s}\}\right) d\mathbf{s}. \end{aligned} \quad (11)$$

Apparently, the second term at the last line of (11) is irrelevant to **b**, so eq. (11) could be further simplified to

$$\mathcal{Q}\left(\mathbf{b}, \hat{\mathbf{b}}^{(l)}\right) = \int_{\mathbf{s}} \Pr\{\mathbf{s}|\mathbf{r}, \hat{\mathbf{b}}^{(l)}\} \ln\left(\Pr\{\mathbf{r}|\mathbf{s}, \mathbf{b}\}\right) d\mathbf{s}. \quad (12)$$

By substituting (10) into (12), we could obtain the final formulation of E-step, which is given by

$$\mathcal{Q}\left(\mathbf{b}, \hat{\mathbf{b}}^{(l)}\right) = \Re\left\{\sum_{k=1}^{D} r_k \zeta_k^*\left(\mathbf{r}, \hat{\mathbf{b}}^{(l)}\right) \exp(-j\phi_k)\right\}, \quad (13)$$

where ζ_k is the *a posteriori* expectation of the kth symbol, which is given by

$$\zeta_k\left(\mathbf{r}, \hat{\mathbf{b}}^{(l)}\right) = \sum_{s_k \in \mathcal{S}} s_k \Pr\{s_k|\mathbf{r}, \hat{\mathbf{b}}^{(l)}\}. \quad (14)$$

Based on (13), the M-step of EM algorithm could be obtained, which is given by

$$\hat{\mathbf{b}}^{(l+1)} = \arg\max_{\mathbf{b}} \Re\left\{\sum_{k=1}^{D} r_k \zeta_k^*\left(\mathbf{r}, \hat{\mathbf{b}}^{(l)}\right) \exp(-j\phi_k)\right\}. \quad (15)$$

By substituting $\phi_k = 2\pi k \Delta f T_s + \theta$ into (13), (13) is specified as

$$\mathcal{Q}\left(\mathbf{b}, \hat{\mathbf{b}}^{(l)}\right)$$
$$= \Re\left\{\sum_{k=1}^{D} r_k \zeta_k^*\left(\mathbf{r}, \hat{\mathbf{b}}^{(l)}\right) \exp(-j2\pi k \Delta f T_s) \exp(-j\theta)\right\}. \quad (16)$$

According to (16), (15) is further specified as

$$\Delta \hat{f}^{(l)} = \arg\max_{\Delta f} \left|\sum_{k=1}^{D} r_k \zeta_k^*\left(\mathbf{r}, \hat{\mathbf{b}}^{(l-1)}\right) \exp(-j2\pi k \Delta f T_s)\right|, \quad (17)$$

$$\hat{\theta}^{(l)} = \arg\left\{\sum_{k=1}^{D} r_k \zeta_k^*\left(\mathbf{r}, \hat{\mathbf{b}}^{(l-1)}\right) \exp(-j2\pi k \Delta \hat{f}^{(l)} T_s)\right\}, \quad (18)$$

which finally clarifies the EM solutions of the estimations of carrier frequency offset and phase offset.

III. SYSTEM MODEL

In this section, we concentrate on the uplink signal processing precess of the covert satellite communication system. We propose a polar code aided intelligent signal processing method. Firstly, we construct the system framework. In this step, we design the basic polar code aided carrier synchronization algorithm for the simplest case, where only a single processing branch is considered. Then, we develop the original polar code aided carrier synchronization algorithm and apply it to the multi-stream multi-processing branches architecture. Finally, in order to realize the combination between multi-streams and obtain diversity gain, we exploit polar code again and design the polar code based multiple data stream combination algorithm.

A. INTELLIGENT COVERT SATELLITE COMMUNICATION SYSTEM

1) MULTI-CARRIER INTELLIGENT COVERT COMMUNICATION SYSTEM

In order to enhance the covertness of uplink transmission of satellite communication system, we propose an intelligent covert scheme, which employs the MC-DS-CDMA system as its fundamental framework. The resultant multi-carrier intelligent covert satellite communication (MCICSC) system is shown in Fig. 2 and Fig. 3. Similar to MC-DS-CDMA scheme, MCICSC scheme also employs multiple carriers and spread spectrum techniques. However, the distinct of MCICSC is that it has a spectrum sensing module at the transmitter, which will dynamically adjust the parameters of MCICSC according to the practical electromagnetic environment. Instead of directly parallelizing the original sequential information bits in MC-DS-CDMA system, we repeat an information bit firstly, and then input the copies into parallel data processing branches in our MCICSC. As shown in Fig. 2, the architecture of MCICSC transmitter consists of two components, namely intelligent covert data transmitting module (ICDTM) and environmental electromagnetic wave analyzing module (EWAM).

The main principle for realizing the covertness of our MCICSC system is to overlap our useful signal waveforms on the environmental electromagnetic waveforms.[1] In other words, the conventional communication system always attempt to avoid interferences. However, in contrast, our MCICSC system actively creates interfering scenario and exploits the interference signal to covert the useful messages. Working in this way, the transmitted message is able to perfectly hidden itself under the environmental electromagnetic waves, especially when the power spectrum density (PSD) of the useful message is quite small than that of the environmental electromagnetic waves.

As shown in Fig. 2, EWAM senses the environmental electromagnetic signals, and also estimates their characteristics, including central frequency, effective bandwidth and PSD, *etc*. On the other hand, ICDTM performs the intelligent covert data transmission, according to the parameters feedback from EWAM. In more detail, in ICDTM module, the original data stream is repeated J times and each of the copied data stream will be input into a processing branch (PB). In every PB, the copied data will be consecutively processed by polar encoding, modulation, spectrum spreading, wave shaping, carrier-multiplying and power control. Then the resultant signals of all the branches are further combined into a single MCICSC symbol by a multiplexer. This MCICSC symbol is sent to the channel.

---

[1]The overlapping here means the power spectrums of useful signal and that of the existing interference signal have large common parts. Ideally, their central frequency should be the same. Furthermore, the bandwidth of useful signal would exceed that of interference signal if the latter is a narrow-band signal. In this case, the covertness of the useful signal is not good. Therefore, In order to guarantee high covert communication, it is preferred to select wide-band interference signals for realizing in MCICSC.
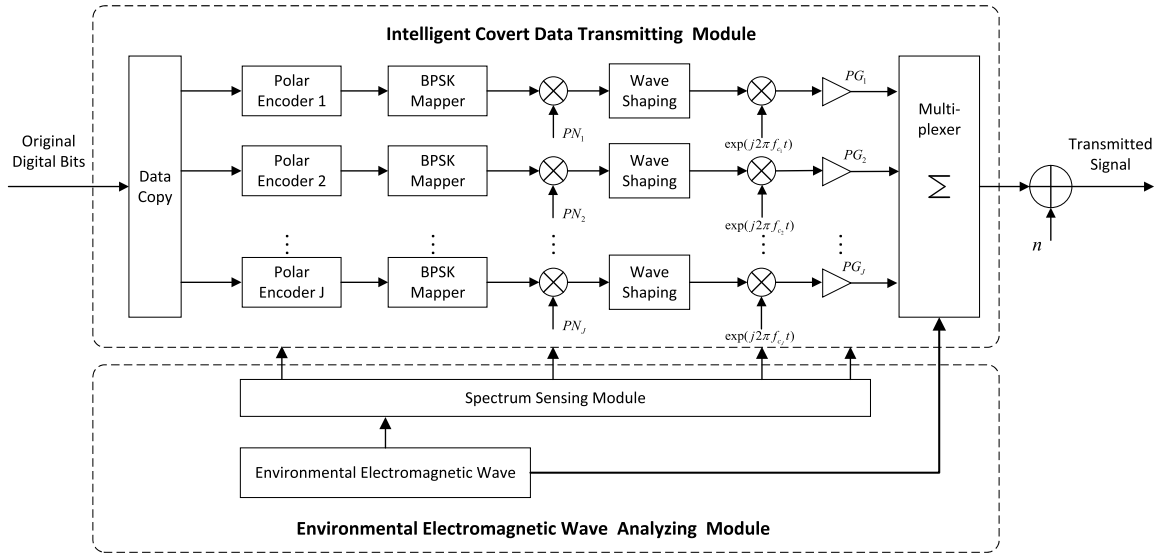
FIGURE 2. Schematic of the transmitter for intelligent covert satellite communications.
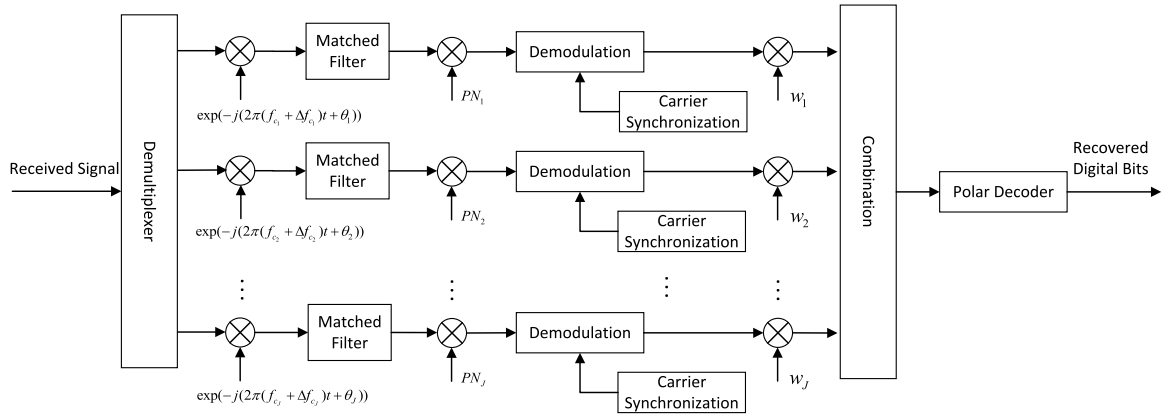

FIGURE 3. Schematic of the receiver for the intelligent covert satellite communications.

According to above descriptions, a MCICSC symbol can be represented as

$$
\begin{aligned}
S_{MCICSC}(t) \\
= \sum_{j=0}^{J-1} \sum_{i=0}^{N-1} \sum_{k=0}^{N_p-1} & \left(b_i^j p_{ik}^j h_{T_c}(t - iT_s - kT_c) G_j \exp\left(j2\pi f_{c_j}t\right) \right. \\
& \left. + N_j(t) \right),
\end{aligned}
\tag{19}
$$

where J is the number of PBs, N is the codeword length, N_p is the PN code length, $b_i^j \in \{\pm 1\}$ denotes the ith BPSK symbol during the jth PB, $p_{ik}^j \in \{0, 1\}$ denotes the kth chip used to spread b_i^j. $h_\tau(t)$ is the chip waveform during the interval of $[0, \tau)$. T_s and T_c represent symbol and chip duration respectively. G_j is the amplification factor of the jth amplifier PG_j in Fig. 2. f_{c_j} is the carrier central frequency employed by jth PB. $N_j(t)$ represents the electromagnetic signal interfering the signal output from the jth PB.

The receiver architecture for MCICSC is shown in Fig. 3. It observed at Fig. 3 that the received signal is firstly

processed by a de-multiplexer, which outputs J signal streams. Then, each single data stream would be successively processed by frequency down-conversion, matched filtering, de-spreading and demodulation. In demodulation step, carrier synchronization is implemented for assisting the demodulation process. The demodulated symbols of all the PB will be combined at the diversity combing module.

In order to cover the original message and simultaneously achieve an acceptable communication quality, each PB of MCICSC has to support flexible configuration of power gain (PG), subcarrier frequencies, pseudo-noise spreading codes, as well as different polar codes. In practical, various intelligent algorithms including Artificial Intelligence can be applied to the configuration process. Benefiting from these intelligent configuration, the MCICSC system could adapt to various practical communication scenarios and achieve a good trade-off among covertness, performance and complexity [43], [44]. In the following description, we would like to address our configuration strategy.

2) GUIDELINES FOR DESIGNING INTELLIGENT COVERT TRANSMISSION

According to the above discussions, three critical metrics should be considered, namely, covertness, performance and complexity.

Firstly, as mentioned in Section I, covertness of communication could be enhanced by reducing the length of data packet. It implies short polar codes have to be employed in each PB. On the other hand, using a low transmission power in each PB also increases the covertness.

Then, we have to improve the system performance on the limitations of a low transmit power and a short codeword length. Accordingly, designing a powerful detection scheme becomes a necessary solution, which could be readily achieved by exploiting our advanced synchronization scheme, and by employing our new diversity combination technique, as well as by invoking the iterative detection architecture.

Finally, let us consider the low complexity issue. Apparently, the short codeword length configuration is inherently in accordance with low computational complexity. But we still need to further reduce the complexity by simplifying the signal synchronization and diversity combination scheme.

The above analyses reveal the principles of designing a good intelligent covert data transmission system. In practice, these guidelines should also adapt to various application scenarios.

B. BASIC POLAR CODE-AIDED CARRIER SYNCHRONIZATION MODEL

In this Section we focus on the carrier synchronization problem of MCICSC. Assume that the entire transmit power of an information bit is fixed. Since an original information bit will be further repeated by J times and these copies will be input in J PBs, the transmit power of any PB may become very low. Furthermore, according to our guidelines addressed in Section III-A.2, we always attempt to couple the output of a PB with a strong interference. Accordingly, each PB has a high probability of working in an extremely low SNR. On the other hand, we will show that polar code is very sensitive to the carrier synchronization error in forthcoming simulations. It means the performance of MCICSC system will rapidly degrade even encountering a slight synchronization error. Thus, the accuracy of carrier synchronization is extremely important. However, achieving a precise synchronization in low SNR scenarios is always a hard challenge. The penalty of the associated solutions is always imposing a prohibitively high computation complexity. Therefore, we have to overcome the carrier synchronization problem of MCICSC system while it operates in a low SNR region.

Inspired by the fact that polar code is capable of working at an extremely low SNR region, we conceived a polar code-aided carrier synchronization model. As stated before, we would first study the single PB case, and then extend
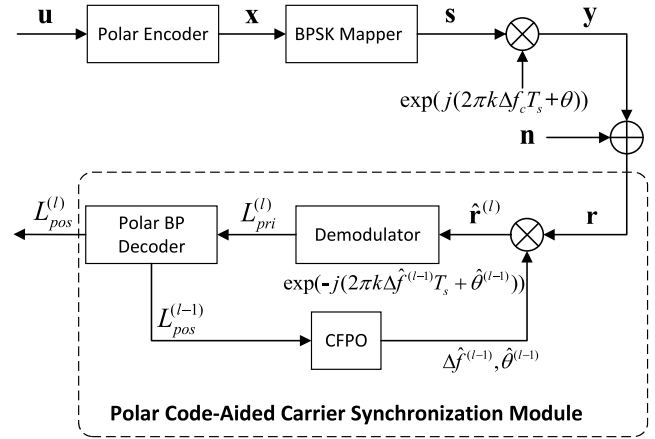

FIGURE 4. Polar code-aided carrier synchronization communication system for a single data stream of MCICSC. CFPO: calculator of frequency and phase offset.

the scheme to multiple PB case in MCICSC system.[2] The proposed polar code-aided carrier synchronization complex baseband model for a single PB case is shown in Fig. 4.

Observe at Fig. 1 that at the transmitter, the original information sequence **u** is firstly encoded by a polar code. Then, the encoded signal **x** is mapped to BPSK symbols. Additionally, we multiply the modulated signal by a complex random signal of $\exp(j(2\pi k \Delta f_c T_s + \theta))$ for modeling the affect of the carrier frequency and phase offsets. Next, we define the following column vectors:

$$\begin{aligned}
\mathbf{u} &= (u_1, u_2, \ldots, u_N)^T \\
\mathbf{x} &= (x_1, x_2, \ldots, x_N)^T \\
\mathbf{s} &= (s_1, s_2, \ldots, s_N)^T \\
\mathbf{y} &= (y_1, y_2, \ldots, y_N)^T \\
\mathbf{n} &= (n_1, n_2, \ldots, n_N)^T,
\end{aligned} \tag{20}$$

which are respectively original data, coded data, modulated symbols, frequency and phase distorted signals, and sampled AWGN vector. N denotes code length. $\mathbf{n} \sim \mathcal{CN}(0, \sigma^2)$ and has a two-side power spectrum density of $N_0 (watts/Hz)$. According to the operations shown in Fig. 4, we have following relations

$$\begin{aligned}
\mathbf{x} &= \mathbf{uG} \\
s_k &= \exp(jx_k \pi) \\
y_k &= s_k \exp(j(2\pi k \Delta f_c T_s + \theta)),
\end{aligned} \tag{21}$$

where $k = 1, 2, \ldots, N$ is time index, Δf_c is carrier frequency offset and θ is carrier phase offset. Thus, based on (21), the received signal is given by

$$r_k = s_k \exp(j(2\pi k \Delta f_c T_s + \theta)) + n_k. \tag{22}$$

Polar code aided carrier synchronization module at the receiver consists of four components: offset compensator,

---

[2]For in this section we mainly study the affect of carrier's frequency and phase offset in MCICSC, it is reasonable to assume that the timing and frame synchronization are ideal at the receiver.
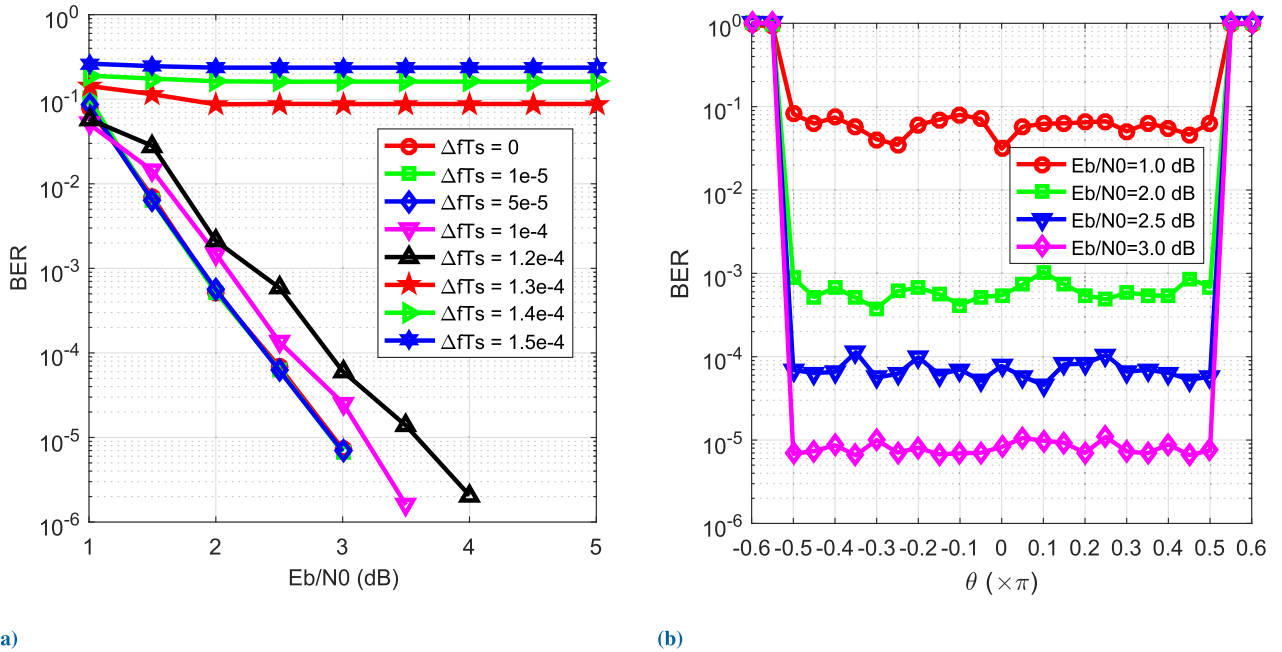
(a)

(b)

FIGURE 5. Ber performance for $C_1(2048, 1024)$ in terms of frequency and phase offset: (a). Ber performance with different frequency offset and zero phase offset; (b). Ber performance with different phase offset and zero frequency offset.

which is denoted by the multiplier label within the dashed block of Fig. 4; demodulator; the polar code BP decoder; as well as the calculator of frequency and phase offset (CFPO). As observed in Fig. 4 that these four components will work in an iterative manner. In more detail, in the lth iteration, the received signal **r** is compensated by the output of CFPO. For the first iteration, the offsets of frequency and phase are initialized to zero. Correspondingly, the compensated signal is formulated as

$$\hat{r}_k^{(l)} = \hat{r}_k^{(l-1)} \exp(-j(2\pi k \Delta \hat{f}^{(l-1)} T_s + \theta^{(l-1)})). \quad (23)$$

Then the demodulator performs soft BPSK demodulation process based on $\hat{\mathbf{r}}$. The BPSK soft demodulator outputs the *a priori* log-likelihood ratio (LLR) information of $L_{pri}^{(l)}$ to the polar decoder. Based on the *a priori* information and employing the BP algorithm as the decoding algorithm, the polar decoder could further generate the *a posteriori* LLR of $L_{pos}^{(l)}$. More specifically, the BP algorithms of polar code can be categorized into generator matrix based BP (G-based BP) and parity-check matrix based BP (H-based BP). But, it was reported in [22] that H-based BP considerably outperforms G-based BP. Meanwhile, the encoding algorithms of polar code can be categorized into systematic encoding and non-systematic encoding. However, it was reported in [45] that, systematic polar code significantly outperforms its non-systematic counterpart. Based on the above analysis, we will employ the systematic polar codes and H-based BP decoding algorithm in support of our MCICSC system. Then, the *a posteriori* information acquiring from the polar decoder will be provided to the CFPO module. With the aid of these *a posteriori* information, CFPO could improve its previous estimations of the frequency offset $\Delta \hat{f}^{(l-1)}$ and

the phase offset $\Delta \theta^{(l-1)}$. Apparently, after forwarding these refined estimation to the offset compensator module, the performance of the soft demodulator will be further enhanced. Hence, the entire system performance will be constantly improved by executing these iterations until the polar code detection passes all the check functions or the maximum iteration number is achieved.

Before further investigating the proposed polar code-aided carrier synchronization scheme, we would firstly demonstrate that short length polar code is very sensitive to the carrier synchronization errors. For an example, in Fig. 5 the bit error rate (BER) curves of systematic polar code $C_1(2048, 1024)$ using H-based BP decoding is demonstrated, where the effect of different frequency and phase offsets are investigated. In Fig. 5(a), we observe that while the level of normalized frequency offset $\Delta f T_s$ is less than 10^{-5}, there is almost no performance loss. But the performance degrades rapidly after the frequency offset exceeds a level of 1.2×10^{-4}. Furthermore, it does not work any more when the frequency offset is larger than 1.3×10^{-4}. On the other hand, Fig. 5(b) shows the BER performance of C_1 with different phase values. It demonstrates that while the E_b/N_0 is greater than 2dB the BER is less than 10^{-3} within the phase offset range of $[-0.5\pi, 0.5\pi]$. However, while exceeding this range the performance dramatically degrades again. Finally, the BER performance will become much worse if both frequency offset and phase offset exist. Therefore, carrier synchronization is a critical module for MCICSC system.

Moreover, the most critical step for realizing an accurate carrier synchronization is the CFPO module. As stated before, the CFPO performance is optimized by exploiting EM algorithm. According to (17) and (18), the fundamental

of EM algorithm is obtaining the expectation of transmit symbols. In more detail, the *a posteriori* LLR of the kth bit of a symbol $\mathbf{x}$ is given by

$$L_{pos}^{(l)}(x_k) = \ln \frac{\Pr\{x_k = 0|\hat{r}_k^{(l)}\}}{\Pr\{x_k = 1|\hat{r}_k^{(l)}\}}. \tag{24}$$

In the CFPO module, at lth iteration it will calculate the frequency and phase offset of the carrier based on the received signals $\hat{\mathbf{r}}^{(l)}$ and the *a posteriori* information $L_{pos}^{(l)}$ acquired from polar decoder. According to (14), EM requires the expectations of all modulated symbol $s_k, k = 1, 2, \ldots, N$. Without loss of generality, for the BPSK modulation, we have

$$\Pr\{s_k = \exp(j \cdot 0 \cdot \pi)|\hat{r}_k\} = \Pr\{x_k = 0|\hat{r}_k\}, \tag{25}$$

and

$$\Pr\{x_k = 0|\hat{r}_k\} + \Pr\{x_k = 1|\hat{r}_k\} = 1. \tag{26}$$

According to (24), (25) and (26) the probability of $s_k = \exp(j \cdot 0 \cdot \pi)$ on condition of $\hat{r}_k$ is written as

$$\Pr\{s_k = \exp(j \cdot 0 \cdot \pi)|\hat{r}_k\} = \frac{\exp(L_{pos}(x_k))}{\exp(L_{pos}(x_k)) + 1}. \tag{27}$$

Similarly, the probability of $s_k = \exp(j \cdot 1 \cdot \pi)$ on condition of $\hat{r}_k$ is given by

$$\Pr\{s_k = \exp(j \cdot 1 \cdot \pi)|\hat{r}_k\} = \frac{1}{\exp(L_{pos}(x_k)) + 1}. \tag{28}$$

Hence, the expectation of symbol s_k could be derived as follows

$$
\begin{aligned}
\zeta_k &= \exp(j \cdot 0 \cdot \pi) \cdot \Pr\{s_k = \exp(j \cdot 0 \cdot \pi)|\hat{r}_k\} \\
&\quad + \exp(j \cdot 1 \cdot \pi) \cdot \Pr\{s_k = \exp(j \cdot 1 \cdot \pi)|\hat{r}_k\} \\
&= 1 \cdot \frac{\exp(L_{pos}(x_k))}{\exp(L_{pos}(x_k)) + 1} + (-1) \cdot \frac{1}{\exp(L_{pos}(x_k)) + 1} \\
&= \frac{\exp(L_{pos}(x_k)) - 1}{\exp(L_{pos}(x_k)) + 1} = \tanh\left(\frac{L_{pos}(x_k)}{2}\right),
\end{aligned}
\tag{29}
$$

where tanh is hyperbolic tangent function and $\tanh(x) = \frac{\exp(x) - \exp(-x)}{\exp(x) + \exp(-x)}$. Furthermore, in order to reduce the computational complexity of tanh, a linear piecewise function can be used and (29) can hence be approximated as

$$
\zeta_k \approx \begin{cases}
1, & L_{pos}(x_k) > Th \\
\alpha L_{pos}(x_k), & -Th < L_{pos}(x_k) \leq Th \\
-1, & L_{pos}(x_k) \leq -Th,
\end{cases}
\tag{30}
$$

where α and Th are the linear factor and threshold value, respectively. In order to achieve a precise approximation of tanh, α and Th may be specified as $\alpha = 1/3$ and $Th = 3$. The polar code-aided carrier synchronization algorithm relying on (29) and (30) are termed as the *polar code-aided algorithm* (PCAA) and the *simplified polar code-aided algorithm* (S-PCAA), respectively.

Thus, the steps of the proposed PCAA (or S-PCAA) are summarized as follows:

Step 1): Initialize the frequency offset and phase offset for the first iteration;

Step 2): Compensate the offsets of frequency and phase according to (23);

Step 3): Demodulate the compensated signal and input the *a priori* information for polar decoder;

Step 4): Implement the H-based BP decoding process and generate the expectations of every symbols according to (29) or (30);

Step 5): Update the frequency offset and phase offset in CFPO by substituting the symbol expectations to (17) and (18);

Step 6): If the number of iteration reaches its maximum value, the algorithm is terminated. Otherwise go back to step 2).

In order to estimate the effectiveness of the proposed polar code-aided carrier synchronization scheme, the associated frequency and phase synchronization mean estimated value (MEV) performance, are demonstrated in Fig. 6 and Fig. 7, respectively. Three kinds of polar codes, namely, $\mathcal{C}_1(2048, 1024)$, $\mathcal{C}_2(1024, 512)$ and $\mathcal{C}_3(512, 256)$ are employed in these simulations. Those codes are constructed in the same way as in [46]. Monte Carlo simulations of 10000 samples are performed at E_b/N_0 of 2.5dB. As observed in Fig. 6(a) that for $\mathcal{C}_1$, frequency offset estimation precision normalized by T_s has approached a level of 10^{-4}. Particularly, while the practical normalized frequency offset is constraint to $[-1.5 \times 10^{-4}, 1.5 \times 10^{-4}]$, an extremely reliable synchronization is achieved. Meanwhile, as observed in Fig. 6(b) that for $\mathcal{C}_1$, phase offset estimation achieves a very high precision as well. In particular, while the phase offset is constraint to $[-0.4\pi, 0.4\pi]$, an extremely reliable synchronization can be guaranteed. Additionally, the performance of PCAA and S-PCAA are almost the same. Hence we could use S-PCAA algorithm in the rest of the paper for reducing complexity but without loss of performance. Furthermore, in Fig. 7 it can show that as the code length decreases, the frequency offset estimation almost keeps the same precious level. However, the extremely reliable synchronization range could be further extended. While considering the phase offset synchronization, $\mathcal{C}_2$ and $\mathcal{C}_3$ almost have the same performance.

In order to verify the superiority of our polar code-aided carrier synchronization scheme, namely S-PCAA, we compare the root mean square error (RMSE) performance of our S-PCAA scheme with that of other class carrier synchronization schemes, including the modified Cramer-Rao bound (MCRB) [47], the Fitz frequency offset estimation algorithm [48], as well as the V&V phase offset estimation algorithm [49]. The RMSE of frequency offset estimation is compared in Fig. 8(a), while the RMSE of phase offset estimation is compared in Fig. 8(b). For the fairness, the symbol rate involved in these comparisons remains the same. As observed at Fig. 8(a) that, while focusing on the frequency offset estimation, our S-PCAA scheme always approaches a lower RMSE level compared to the Fitz Estimation scheme regardless of the codeword length. Our scheme also gets more closer to the theoretical MCRB bound. Similar comparison results
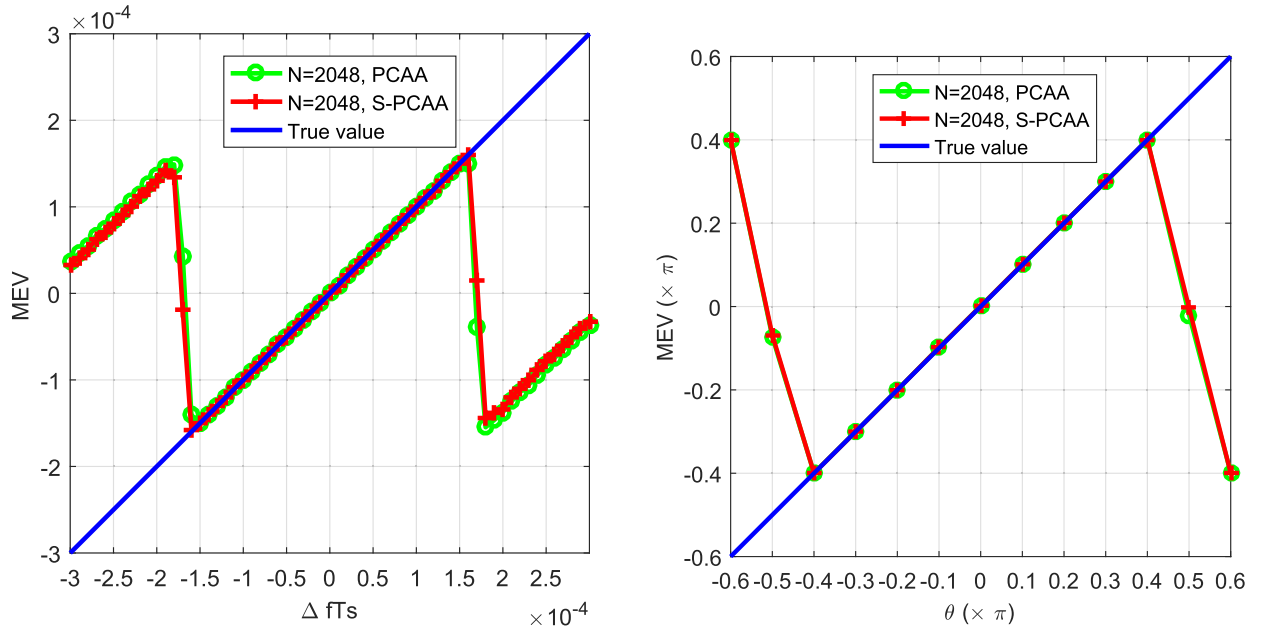
FIGURE 6. MEV curve for $\mathcal{C}_1(2048, 1024)$ in terms of frequency and phase offset: (a). MEV of frequency offset estimation; (b). MEV of phase offset estimation.
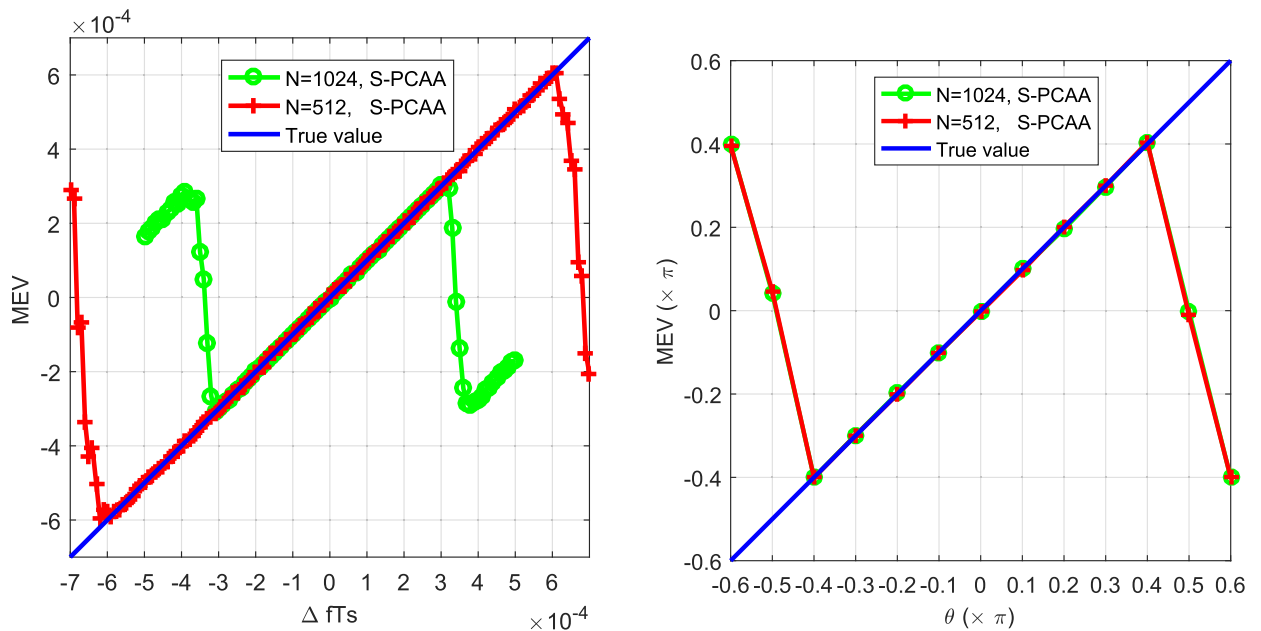
FIGURE 7. Curve of frequency and phase offset for $\mathcal{C}_2(1024, 512)$ and $\mathcal{C}_3(512, 256)$: (a). MEV of frequency offset estimation; (b). MEV of phase offset estimation.

are observed at Fig. 8(b), where we focus on the phase offset estimation.

Therefore, it can be concluded that the polar code-aided carrier synchronization scheme outperforms the traditional synchronization methods. Hence the S-PCAA scheme is employed in our MCICSC system.

C. POLAR CODE-AIDED MULTI-STREAM PARALLEL FEEDBACK CARRIER SYNCHRONIZATION

In the last subsection, the advance of our polar code aided carrier synchronization method is verified. However, it only processes a single data stream. In MCICSC system, we normally encounter multiple data stream case. Hence, we develop the
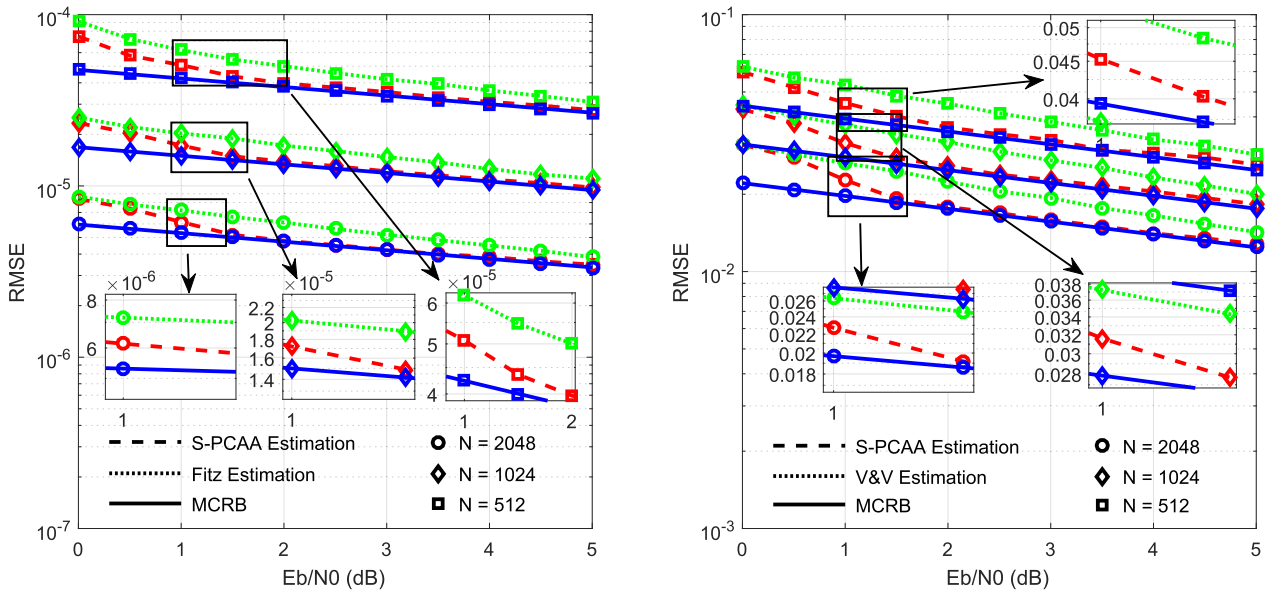
(a)   **(b)**

FIGURE 8. Curves of frequency and phase offset for $C_1(2048, 1024)$, $C_2(1024, 512)$ and $C_3(512, 256)$: (a). RMSE of frequency offset estimation for C_1, C_2 and C_3 having $\Delta f T_s = 1.2 \times 10^{-4}$, 2.5×10^{-4} and 5×10^{-4}; (b). RMSE of phase offset estimation for C_1, C_2 and C_3 having $\theta = 0.2\pi$.
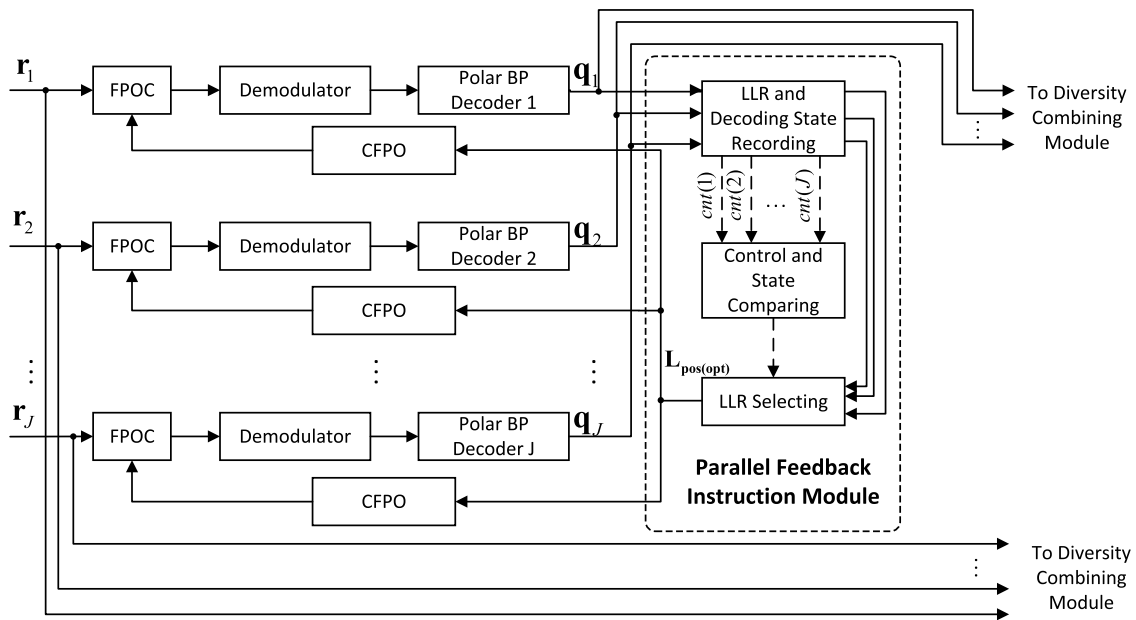

FIGURE 9. Architecture for polar code-aided multi-stream parallel feedback carrier synchronization. FPOC: frequency and phase offset compensator; CFPO: calculator of frequency and phase offset.

S-PCAA scheme in this subsection for satisfying the multiple data stream scenario.

In our MCICSC system, every data stream actually carries the same information. But each data stream will experience independent fading channels. According to the selective combination rule, the *a posteriori* LLRs feedback from the most reliable data stream can be identified, and then be exploited for updating all the CFPO modules. This scheme is capable of acquiring the multiple-stream diversity gain without incurring overly complex data-stream operations.

Inspired by this idea, the polar code-aided multi-stream parallel feedback (PAMSPF) carrier synchronization architecture is constructed, which is depicted in Fig. 9.

Firstly, each data stream $\mathbf{r}_j = (r_{j1}, r_{j2}, \ldots, r_{jN}), j = 1, 2, \ldots, J$ would be compensated by its associated FPOC module, where the frequency offset $\Delta \hat{f}_j^{(l)}$ and phase offset $\hat{\theta}_j^{(l)}$ from CFPO module is formulated as

$$\hat{r}_{jk}^{(l)} = \hat{r}_{jk}^{(l-1)} \exp(-j(2\pi k \Delta \hat{f}_j^{(l-1)} T_s + \theta_j^{(l-1)})). \quad (31)$$

Then, the compensated $\hat{\mathbf{r}}_j$ is demodulated and decoded by the demodulator and the polar BP decoder, respectively. In more detail, in order to adapt to parallel feedback instruction module, H-based BP decoding algorithm is adopted, since it is able to indicate the number of parity check equations that are satisfied during the decoding process. Accordingly, we employ the number of failed parity check equations $cnt(j)$ to measure the reliability of every specific data stream.

On the next step, the detected information $\mathbf{q}_j$ consisting of the *a posteriori* LLRs $\mathbf{L}_j$ and the data stream reliability indicator of $cnt(j)$ will propagate through parallel feedback instruction module.

As shown in Fig. 9, the parallel feedback instruction module plays the role of generating the optimal LLR $\mathbf{L}_{\mathbf{pos(opt)}}$ that will be provided to all the CFPO modules.

Firstly, the LLRs and decoding state recording module receives and caches $\mathbf{q}_j$.

Then, the control and state comparing module will check whether the iteration number approaches a threshold of *IterTh* (*IterTh* is less than the preset maximum iteration number *IterOuter*). The check result is forwarded to the LLR selecting module. If the iteration number has already approached the *IterTh*, it will inform the control and state comparing module. Then, the control and state comparing module will terminate the comparison of the decoding states $cnt(j), j = 1, 2, \ldots, J$ and output the minimum cnt value to the LLR selecting module; otherwise, the LLR and decoding state recording module will not trigger the control and state comparing module and just forward the cached LLRs to the LLR selecting module.

Finally, according to the output of the control and state comparing module, the LLR selecting module would select the optimal LLR $\mathbf{L}_{\mathbf{pos(opt)}}$ and outputs it to all the CFPO modules for updating frequency and phase offset estimation. Before the iteration number reaches *IterTh*, the value of $\mathbf{L}_{\mathbf{pos(opt)}}$ is given by the average LLRs of all the J data streams. However, while the iteration number is equal and greater than *IterTh*, two generation methods of $\mathbf{L}_{\mathbf{pos(opt)}}$ will be opted for. If the minimum cnt value is greater than *CntTh* (a pre-defined value), $\mathbf{L}_{\mathbf{pos(opt)}}$ is still given by the average LLRs of all the J data streams; otherwise, it is given by the LLRs from the most reliable data steam, which achieves the minimum cnt value.

Furthermore, on the condition of employing the BPSK modulation, in each CFPO, after substituting $\mathbf{L}_{\mathbf{pos(opt)}}$ into (30), we will obtain a more accurate symbol expectation. As a result, the EM algorithm implemented in each CFPO will achieve a fast convergence. Then, we can generate the frequency and phase offset according to (17) and (18) which will feedback to FPOC modules. Now we have completed one iteration of polar code-aided multi-stream parallel feedback carrier synchronization for MCICSC. Repeating all the above processes until the synchronization iteration reaches *IterOuter*, we could output the $\mathbf{q}_j, j \in \{1, 2, \ldots, J\}$ to the concatenated diversity combing module.

According to the above description, in our parallel feedback mechanism, we do not feedback the LLR $\mathbf{L}_{\mathbf{pos(j)}}$, which comes from the data stream achieving the minimum value of $cnt(j)$ among $(cnt(1), cnt(2), \ldots, cnt(J))$, in the early iterations. Instead, we feedback the average LLRs collected from all the data-streams. Because each PB normally works in a very low SNR range in our MCICSC system. It implies the LLRs of all the data stream can not reach their static states in the early iterations. Hence it has a high probability that the data stream does not experience the best channel even it achieves a temporary minimum value of $cnt(j)$. Obviously, this conflict may further impair the synchronization performance of the forthcoming iterations. Accordingly, in order to avoid utilizing unreliable LLR information, we set a threshold of iteration number. Before reaching this threshold, we always utilize the average LLRs of all the data streams. After the iteration number approaches the threshold, we have to make decision: continuously use the average LLRs or begin to use the LLRs from the best data stream. we set the threshold of *IterTh* to 10 in our simulations, while the maximum iteration number is 20.

Another critical issue is determining an appropriate value of *CntTh*, which is regarded as the criterion for triggering the LLR selecting module to utilize the LLRs from the best data-stream. It is clear that the confidence level of LLR is proportional to SNR, meanwhile the value of cnt is inversely proportional to SNR. Hence, the smaller the cnt is, the higher the confidence level of LLR increases. In this spirit, at the 10th iteration, we run a Monte Carlo simulation for evaluating the probability mass function (PMF) and cumulative density function (CDF) of cnt value of a single data stream, where various E_b/N_0 values are tested. For guaranteeing the simulation accuracy, the Monte Carlo simulation is terminated until 500 erroneous frames are observed. The simulation result is shown in Fig. 10.

It can be seen in Fig. 10 that the PMFs of cnt value are very similar within the E_b/N_0 region of -3dB, -5dB and -8dB, while that of 0dB is quite different. For example, The CDF of the event that the cnt value is lower than 900 is around 18%, while the E_b/N_0 equals to 0dB. In contrast, the CDF almost drops to zero, while E_b/N_0 equals to -8dB, -5dB and -3dB. Hence, in this case, the *CntTh* of 900 can effectively achieve the goal of distinguishing the most reliable data stream from other data streams. The MCICSC system benefits from this specification method of *CntTh*, which will be demonstrated in Section IV. Furthermore, it is noticing that the above mentioned principle of determining the *CntTh* value is a generalized method.

The pseudo code for the proposed synchronization algorithm is shown in the Algorithm 1. The performance of this algorithm will be shown in Section IV. In next subsection, we would continue to discuss another significant issue of MCICSC, namely, diversity combining.
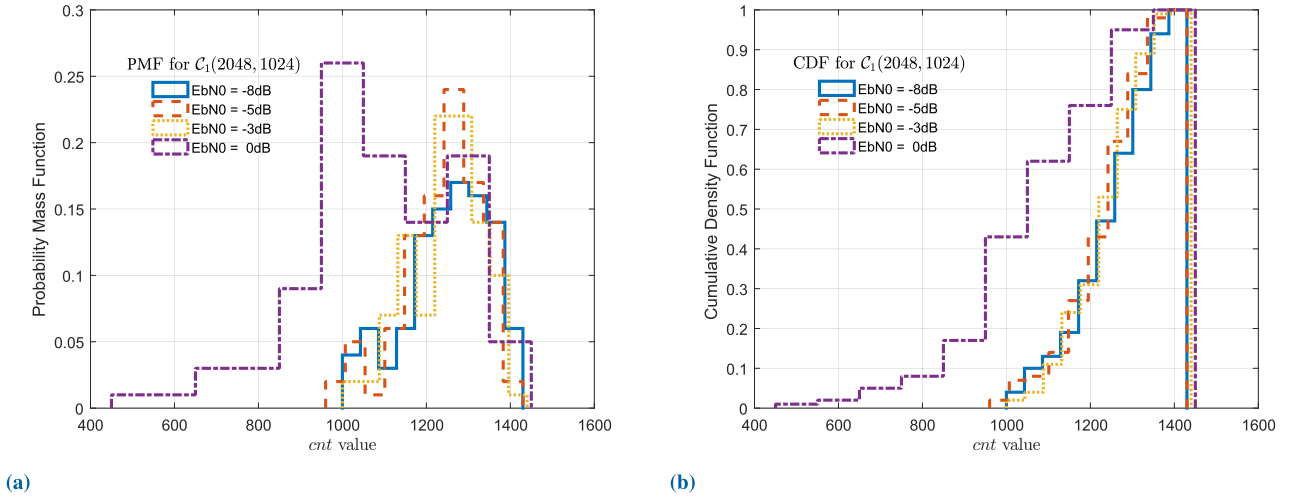
FIGURE 10. Statistics curves for the *cnt* value of $\mathcal{C}_1(2048, 1024)$ with different E_b/N_0: (a). PMF of *cnt* value with frequency offset $\Delta fTs = 5.0 \times 10^{-5}$ and phase offset $\theta = 0.2\pi$; (b). CDF of *cnt* value with frequency offset $\Delta fTs = 5.0 \times 10^{-5}$ and phase offset $\theta = 0.2\pi$.

D. POLAR CODE-BASED DIVERSITY COMBINING ARCHITECTURE

The aim of diversity combining is to obtain an appropriate combination weight coefficient set of $\mathbf{w} = (w_1, w_2, \ldots, w_J)$, which could result in a good BER performance. It is well known that MRC method is the optimal combining method, which requires the channel state information (CSI) of each data stream at the receiver. The traditional channel estimation could be categorized into data-aided method and pilot aided method. However, they either impose extra computational complexities or require extra overhead of channel resources. In order to achieve the tradeoff between the performance and the complexity of our MCICSC system, we construct a polar code-based diversity combing (PBDC) architecture as shown in Fig. 11. It is capable of generating the combining coefficients without CSI. Moreover, the PBDC combining method almost imposes no extra resources.

As shown in Fig. 11, the PBDC architecture has two inputs from the carrier synchronization module: one is the final decoding result of each data stream during the *IterOuter*th iteration, which is denoted by $\mathbf{q}^{l_{max}} = (\mathbf{q}_1^{l_{max}}, \mathbf{q}_2^{l_{max}}, \ldots, \mathbf{q}_J^{l_{max}})$; the other is the carrier synchronized signal, which is indicated by $\mathbf{r} = (\mathbf{r}_1, \mathbf{r}_2, \ldots, \mathbf{r}_J)$. Based on $\mathbf{q}^{l_{max}}$, the Combining Strategy Generating Module (CSGM) generates the combination coefficients of $\mathbf{w} = (w_1, w_2, \ldots, w_J)$. Based on the combination coefficients, the combined signal to be decoded can be expressed as

$$\mathbf{r_{comb}} = \sum_{j=1}^{J} w_j \mathbf{r}_j. \tag{32}$$

The algorithm employed by our CSGM module for generating an appropriate weight set of $\mathbf{w}$ is stated in the next paragraph.

The CSGM consists of the state deciding component and the combing coefficient calculating component. In more detail, in the stating deciding component, if $cnt(j)$ equals to 0,

the coefficient w_j associated with that data stream is set to 1. Otherwise, the coefficient w_j is set to 0. The condition that all the $cnt(j), j = 1, 2, .., J$ are larger than 0 will trigger the combining coefficient calculating component. In this particular case, two steps are implemented in combining coefficient calculating component. The first step is to normalize each $cnt(j)$ value by the sum of all cnt values, which could be formulated as

$$p(j) = \frac{cnt(j)}{\sum_{m=1}^{J} cnt(m)}, \quad j \in \{1, 2, \ldots, J\}. \tag{33}$$

The second step is to calculate coefficients w_j according to

$$w_j = 1 - p(j), \quad j \in \{1, 2, \ldots, J\}. \tag{34}$$

(33) and (34) are designed based on the straightforward principle that assigning a larger weight to the more reliable data stream during the combination process. The integrated pseudo codes of the proposed polar coded-based diversity combing algorithm is shown in Algorithm 2. The performance and complexity analysis will be presented in Section IV.

IV. SIMULATION RESULTS

Numerous simulation results of the carrier synchronization and diversity combing schemes proposed for our MCICSC system are demonstrated in this section.

We construct polar codes according to the same method in [46], which is applied to all the PB modules. Modulation scheme is fixed to BPSK. Furthermore, without loss of generality, fixed normalized frequency offset and phase offset are employed during all the simulations. The detailed simulation parameters employed are listed in Table 1.

Firstly, in order to demonstrate the superiority of PAMSPF algorithm compared with Direct Parallel Method which independently employs the S-PCAA estimation on all data streams, RMSE curves versus E_b/N_0 of frequency and phase offset for $\mathcal{C}_1$ are shown in Fig. 12. The RMSE performances

---

Algorithm 1 Polar Code-Aided Multi-Stream Parallel Feedback Carrier Synchronization Algorithm

Input:

$\mathbf{r}_j, j = 1, 2, \ldots, J$: J data streams after despreading;

IterOuter: Maximum synchronizing iteration number;

IterInner: Maximum polar BP decoding iteration number.

Output:

$\mathbf{q} = (\mathbf{q}_1, \mathbf{q}_2, \ldots, \mathbf{q}_J)$: Detected information sequence;

$\mathbf{L_{pos}}_j$ and $cnt(j)$ denote the *a posteriori* LLRs and reliability indicator of jth data stream, respectively.

Note: $\mathbf{q}_j = [\mathbf{L_{pos}}_j, cnt(j)]$.

// Initialize Δf and θ

1: **for** j = 1 : J **do**
2:    $\Delta \hat{f}_j^{(0)} = 0, \hat{\theta}_j^{(0)} = 0$;
3: **end for**
   // Main loop
4: $l = 1$;
5: **while** ($l \leq IterOuter$) **do**
6:    **for** j = 1 : J **do**
7:       Update $\hat{\mathbf{r}}_j^{(l)}$ based on (31);
8:    **end for**
9:    For each data stream, based on $\hat{\mathbf{r}}_j^{(l)}$, perform processes of demodulating and polar BP decoding (the maximum iteration number is *IterInner*), and we would obtain $\mathbf{q}_j^{(l)} = [\mathbf{L_{pos}}_j^{(l)}, cnt(j)^{(l)}], j \in \{1, 2, \ldots, J\}$;
10:    Cache $\mathbf{L_{pos}}_j^{(l)}$ and $cnt(j)^{(l)}$ separately for future use;
   // Find the optimum index of $\mathbf{L_{pos(opt)}}$
11:    **if** $l < IterTh$ **then**
12:       $\mathbf{L_{pos\_sum}} = 0$;
13:       **for** j = 1 : J **do**
14:          $\mathbf{L_{pos\_sum}} = \mathbf{L_{pos\_sum}} + \mathbf{L_{pos}}_j^{(l)}$;
15:       **end for**
16:       $\mathbf{L_{pos(opt)}} = \mathbf{L_{pos\_sum}}/J$;
17:    **else**
18:       *MinValue* $= cnt(1)^{(l)}$;
19:       *index* $= 1$;
20:       **for** j = 2 : J **do**
21:          **if** $cnt(j)^{(l)} < MinValue$ **then**
22:             *index* $= j$;
23:             *MinValue* $= cnt(j)^{(l)}$;
24:          **end if**
25:       **end for**
26:       **if** $MinValue < cntTh$ **then**
27:          $\mathbf{L_{pos(opt)}} = \mathbf{L_{pos}}_{index}$;
28:       **else**
29:          $\mathbf{L_{pos\_sum}} = 0$;
30:          **for** j = 1 : J **do**
31:             $\mathbf{L_{pos\_sum}} = \mathbf{L_{pos\_sum}} + \mathbf{L_{pos}}_j^{(l)}$;
32:          **end for**

Algorithm 1 *(Continued.)* Polar Code-Aided Multi-Stream Parallel Feedback Carrier Synchronization Algorithm

33:          $\mathbf{L_{pos(opt)}} = \mathbf{L_{pos\_sum}}/J$;
34:       **end if**
35:    **end if**
      // Update frequency and phase offset based on the $\mathbf{L_{pos}}$ generated by the above program.
36:    **for** j = 1 : J **do**
37:       Calculate ζ_j based on $\mathbf{L_{pos(opt)}}$ and (30);
38:       Update $\Delta \hat{f}_j^{(l)}$ based on (17);
39:       Update $\hat{\theta}_j^{(l)}$ based on (18);
40:    **end for**
41: **end while**
   // Return the result
42: **for** j = 1 : J **do**
43:    $\mathbf{q}_j = \mathbf{q}_j^{(l)}$;
44: **end for**
45: **return q**;

---

of frequency offset estimation are demonstrated at Fig. 12(a). It is clear that our PAMSPF estimation algorithm always outperforms the traditional direct parallel estimation regardless of the different channel conditions of four data streams. Furthermore, our PAMSPF estimation algorithm is capable of achieving the same performance as that of idealized MCRB algorithm beyond around 4.5dB. While considering the performance of phase estimation, similar phenomenon could be witnessed at Fig. 12(b), where again, our PAMSPF estimation outperforms direct parallel estimation and approaches the performance of MCRB within the high SNR region.

Moreover, in order to verify the generality of the superiority of our PAMSPF algorithm, the RMSE performance comparison associated with other codeword length is simulated. The results are shown in Fig. 13~14. It demonstrated again that the PAMSPF estimation of frequency and phase offset achieves a higher accuracy than direct parallel estimation. It is worth to highlight that with the aid of our PAMSPF algorithm, even the 1st data stream, who experiences the worst channel can be precisely synchronized. The reason is that our PAMSPF algorithm is capable of exploiting the most reliable data stream to improve the synchronization of other data streams.

Then, in order to demonstrate the effectiveness of our PBDC algorithm, we compare its BER performance to that of an idealized MRC algorithm, which has the perfect CSI. In more detail, our PBDC algorithm relies on the signal processing architecture portrayed in Fig. 9 and Fig. 11. Furthermore, in order to concentrate on evaluating the combination algorithm, the asynchronous impact is ignored. It means the perfect synchronization are assumed for both PBDC algorithm and MRC algorithm. The BER performance comparison between our PBDC algorithm and the idealized MRC algorithm is shown in Fig. 15, where three different polar code configurations are involved. As observed in Fig. 15 that for all polar codes configurations, the BER performance discrepancy between our PBDC combination algorithm and
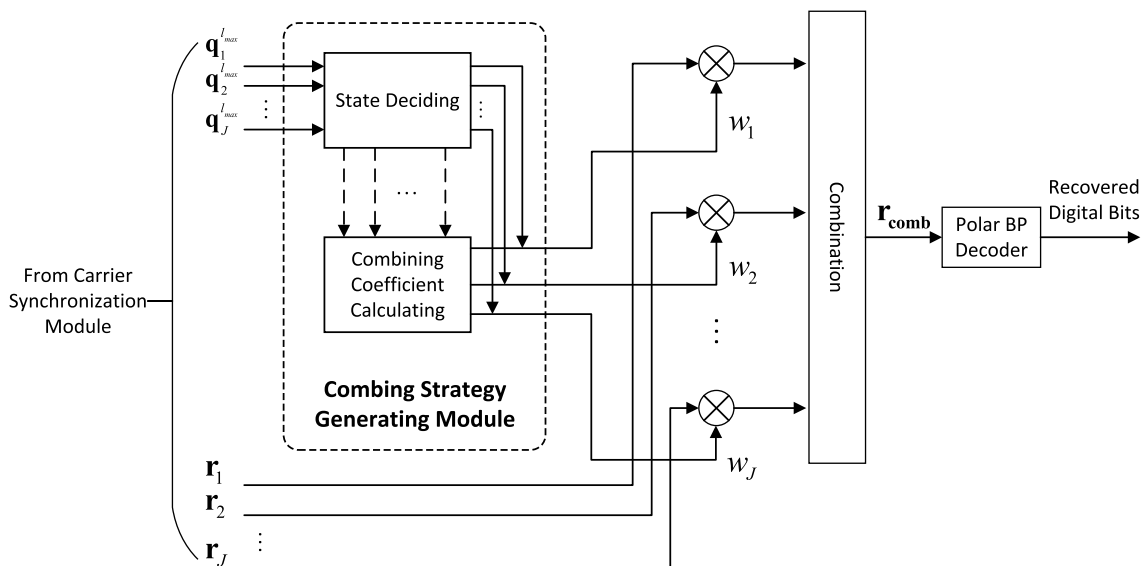
FIGURE 11. Architecture for polar code-based diversity combining.

Algorithm 2 Polar Code-Based Diversity Combining Algorithm

Input:
$\mathbf{q}^{l_{max}} = (\mathbf{q}_1^{l_{max}}, \mathbf{q}_2^{l_{max}}, \ldots, \mathbf{q}_J^{l_{max}})$: Final decoding results input to the process of carrier synchronization;
$\mathbf{L_{pos}}_j$ and $cnt(j)$ denote the *a posteriori* LLRs and reliability indicator of jth data stream, respectively.
Note: $\mathbf{q}_j^{l_{max}} = [\mathbf{L_{pos}}_j, cnt(j)]$.
$\mathbf{r} = (\mathbf{r}_1, \mathbf{r}_2, \ldots, \mathbf{r}_J)$: Output of carrier synchronization module.

Output:
$\mathbf{r_{comb}}$: Combined carrier synchronization signal of J data streams.

1: For each data stream j, cache $cnt(j)$;
      // Calculate weight coefficients
2: **for** j = 1 : J **do**
3:     **if** $cnt(j) == 0$ **then**
4:         **for** k = 1 : J **do**
5:             **if** $k != j$ **then**
6:                 $w_k = 0$;
7:             **else**
8:                 $w_k = 1$;
9:             **end if**
10:         **end for**
11:         $\mathbf{r_{comb}} = \sum_{j=1}^{J} w_j \mathbf{r}_j$;
12:         **return** $\mathbf{r_{comb}}$;
13:     **else**
14:         $p(j) = \frac{cnt(j)}{\sum_{m=1}^{J} cnt(m)}$;
15:         $w_j = 1 - p(j)$;
16:     **end if**
17: **end for**
      // Calculate $\mathbf{r_{comb}}$
18: $\mathbf{r_{comb}} = \sum_{j=1}^{J} w_j \mathbf{r}_j$;
19: **return** $\mathbf{r_{comb}}$;


TABLE 1. Simulation parameters.

Parameter	Specification
Channel	AWGN
Modulation	BPSK
Polar Code configurations	$\mathcal{C}_1, \mathcal{C}_2$ and $\mathcal{C}_3$.
Polar Code type	Systematic Code
Decoding algorithm	H-based BP [25]
Stop criterion used within H-based BP	All parity check equations are satisfied or maximum iteration is exhausted
Normalized frequency offset $\Delta f T s$	5.0×10^{-5} for $\mathcal{C}_1$ 1.0×10^{-4} for $\mathcal{C}_2$ 2.0×10^{-4} for $\mathcal{C}_3$
Phase offset θ	0.2π
Carrier synchronization algorithm	PAMSPF (Algorithm 1) and Direct Parallel Method
Diversity combining algorithm	PBDC (Algorithm 2) and MRC
Max. iteration used in H-based BP	$IterInner = 200$
Max. iteration used between H-based BP and CFPO module	$IterOuter = 20$
Iteration threshold $IterTh$ within Algorithm 1	$IterTh = 10$
Cnt threshold of $cntTh$	900 for $\mathcal{C}_1$ 300 for $\mathcal{C}_2$ 50 for $\mathcal{C}_3$
Number of data streams	$J = 4$
Proportion among the SNRs of four data streams	$1 : 2 : 3 : 6$
Simulation samples	Guarantee that the number of detected erroneous frame > 500

the idealized MRC combination algorithm is always less than 0.5dB. Although, there is a slight performance degradation compared to MRC, our PBDC combination has its particular advantages: a) it does not require the channel estimation, which may become a prohibitive task in some applications; b) its computational complexity is much lower than the MRC algorithm.

Finally, the holistic BER performance of the proposed carrier synchronization scheme concatenated with the PBDC combination algorithm, are demonstrated in Fig. 16, where the impact of practical frequency offset and phase offset is taken into account. Furthermore, the BER performances
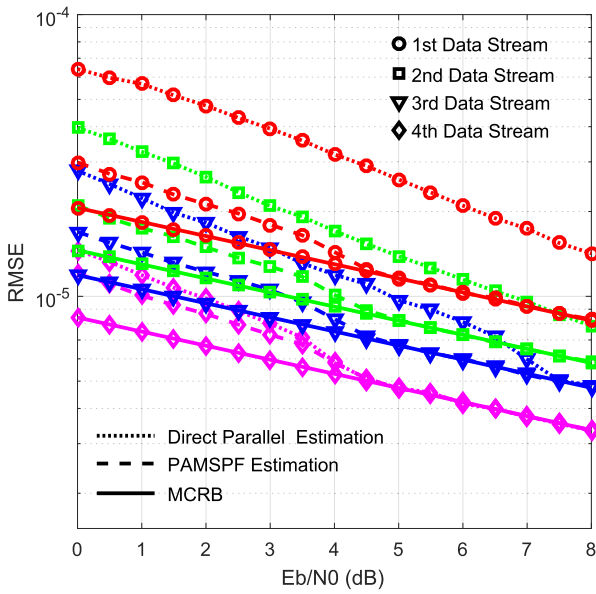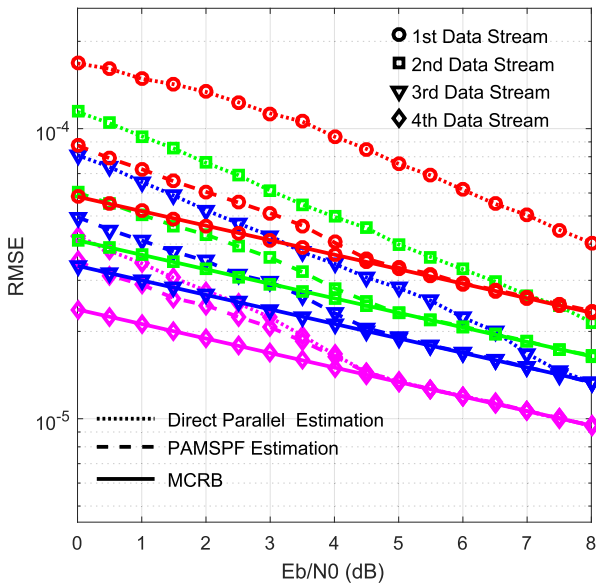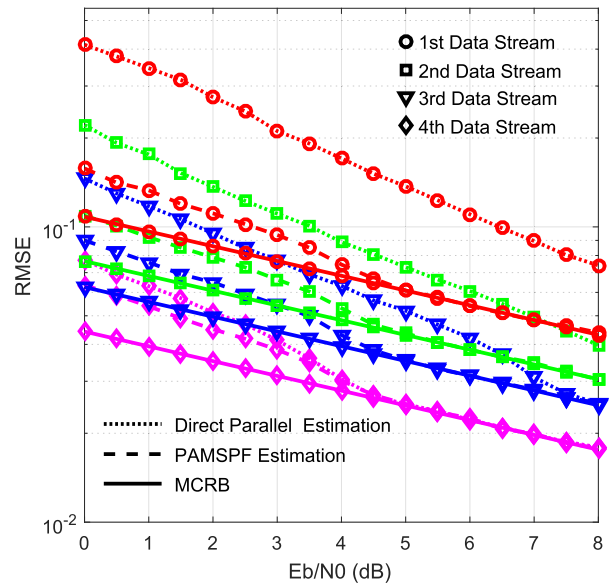
(a)
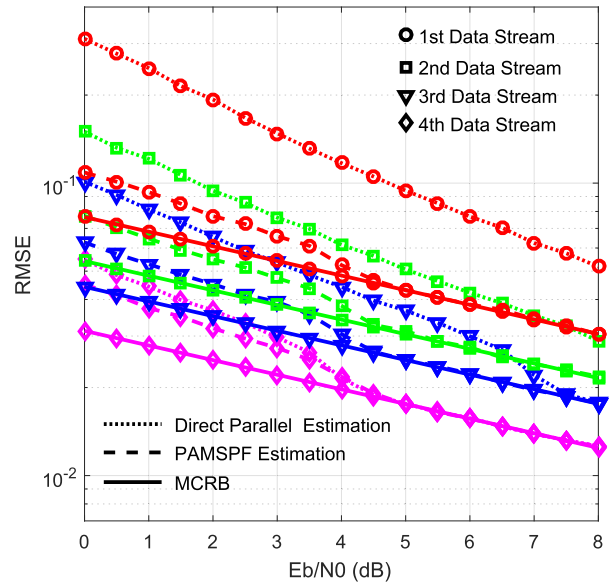
(b)

FIGURE 12. RMSE of the frequency and phase offset estimation in MCICSC system, where the polar code of C_1 (2048, 1024) is employed: (a). RMSE of frequency offset estimation for C_1 while specifying $\Delta fTs = 5.0 \times 10^{-5}$ in MCICSC system; (b). RMSE of phase offset estimation for C_1 while specifying $\theta = 0.2\pi$ in MCICSC system.

(a)

(b)

FIGURE 13. RMSE of the frequency and phase offset estimation in MCICSC system, where the polar code of C_2 (1024, 512) is employed: (a). RMSE of frequency offset estimation for C_2 while specifying $\Delta fTs = 1.0 \times 10^{-4}$ in MCICSC system; (b). RMSE of phase offset estimation for C_2 while having $\theta = 0.2\pi$ in MCICSC system.

of idealized synchronization, direct parallel synchronization, as well as dispensing with synchronization module are employed as our benchmarks. For a fairness, PBDC combination algorithm is employed in all these counterparts. Observed at Fig. 16(a) that while employing the C_1 polar code, the BER performance of our PAMSPF synchronization is almost the same as the idealized synchronization, but an around 0.4dB performance gain is achieved by our

PAMSPF compared with the direct parallel synchronization. After replacing C_1 by either C_2 or C_3, similar performance is observed in Fig. 16(b). In this instance, the performance gain of our PAMSPF algorithm compared to direct parallel synchronization increases to 0.6dB for C_2 and 0.8dB for C_3, respectively. Therefore, it can be concluded that with the aid of the proposed PAMSPF carrier synchronization algorithm and the proposed PBDC combining algorithm, the MCICSC
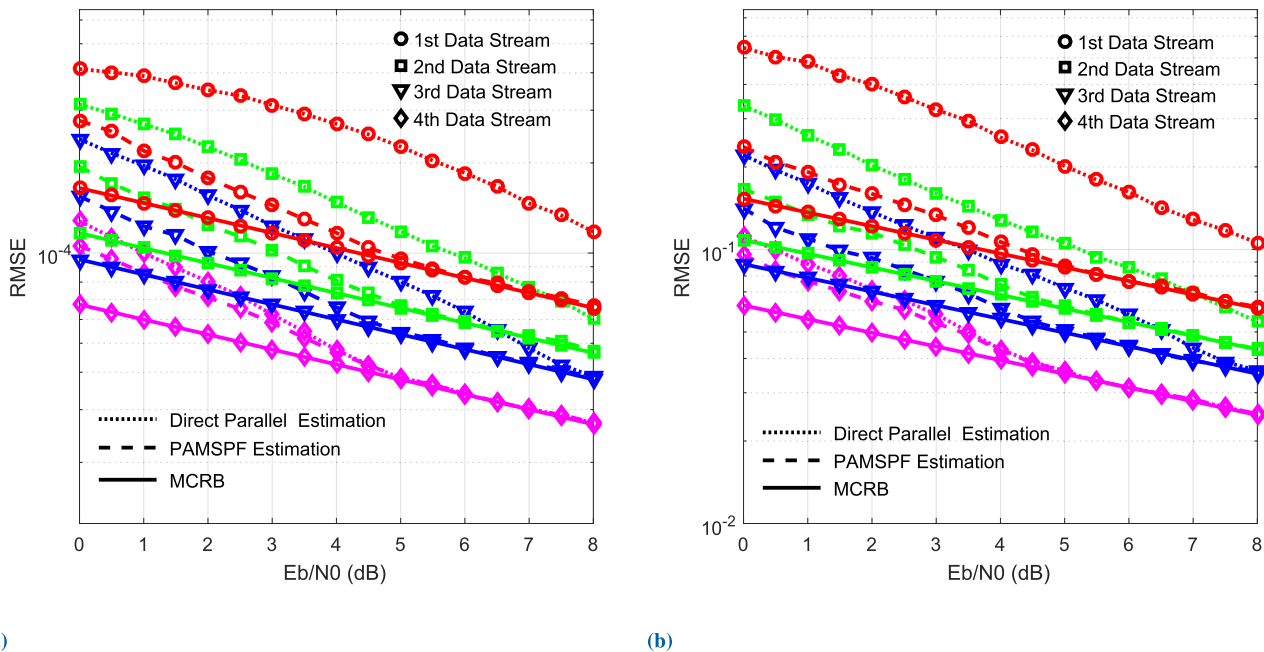
(a)   **(b)**

FIGURE 14. RMSE of the frequency and phase offset estimation in MCICSC system, where the polar code of $\mathcal{C}_3$(512, 256) is employed: (a). RMSE of frequency offset estimation for $\mathcal{C}_3$ while having $\Delta fTs = 2.0 \times 10^{-4}$ in MCICSC system; (b). RMSE of phase offset estimation for $\mathcal{C}_3$ while specifying $\theta = 0.2\pi$ in MCICSC system.
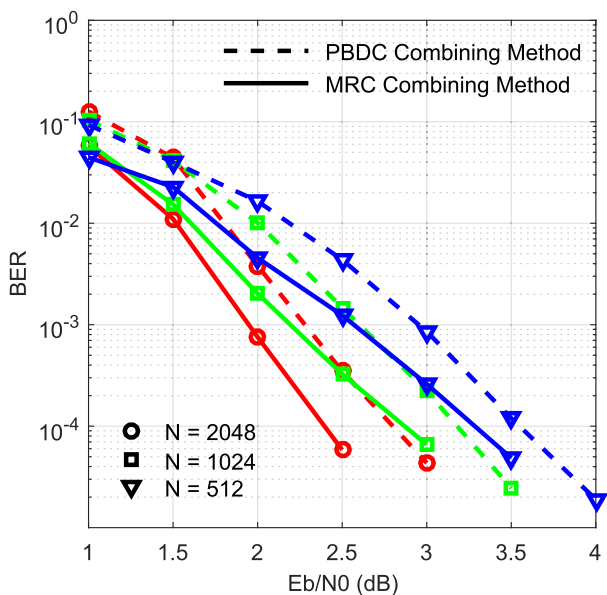

FIGURE 15. BER performance comparison between our PBDC algorithm and the MRC combination in MCICSC system, where three different polar codes of $\mathcal{C}_1$, $\mathcal{C}_2$ and $\mathcal{C}_3$ are involved in this comparison.

system is capable of achieving a high reliability even in a very low SNR region.

V. COMPLEXITY ANALYSIS

The complexity of the proposed carrier synchronization algorithm (PAMSPF) and diversity combination algorithm (PBDC) employed in MCICSC system is analysed in this section. In order to assess the complexity imposed by these two algorithms, the average number of real-valued multiplication and division operation (RMDO) required to

accomplish the carrier synchronization and combining is regarded as our complexity metric.

During the implementation of PAMSPF algorithm, the complexity is mainly imposed by two tasks: a) polar decoding process and CFPO carrier offset calculating process of each data stream; b) Parallel Feedback Instruction Module (PFIM) tackling with all data streams. Hence, the complexity of PAMSPF algorithm could be summarized as

$$\mathcal{C}_{PAMSPF} \approx I_{outer} \left(\sum_{j=1}^{J} (\mathcal{C}_{BP}(j) + \mathcal{C}_{CFPO}(j)) + \mathcal{C}_{PFIM} \right), \quad (35)$$

where $\mathcal{C}_{BP}(j)$ and $\mathcal{C}_{CFPO}(j)$ are the complexity imposed by the polar code BP decoding process and the CFPO carrier offset calculating process of jth data stream, respectively. $\mathcal{C}_{PFIM}$ represents the complexity of PFIM, and I_{outer} denotes the number of actually executed iterations, which equals to the parameter of *IterOuter*. Consecutively, we will individually evaluate $\mathcal{C}_{BP}(j)$, $\mathcal{C}_{CFPO}(j)$ and $\mathcal{C}_{PFIM}$.

Firstly, according to lines 11-35 of Algorithm 1, during every iteration, the PFIM calculation process will require at most N division operations owing to the calculation of $\mathbf{L}_{pos(opt)}$ in line 16 and line 33.

Secondly, for each data stream, the complexity of H-based BP decoding algorithm is dominated by three factors: the codeword length of N, the number of information bits K, the average degree of check nodes $\bar{d}_c$ of the associated parity check matrix H. According to [50], a number of $\mathcal{O}(I_{BP}N(N - K)(\bar{d}_c - 2))$ RMDOs are required for once BP decoding, where I_{BP} records the actually executed iterations within the BP decoding process. It should be less than the parameter of *IterInner*.
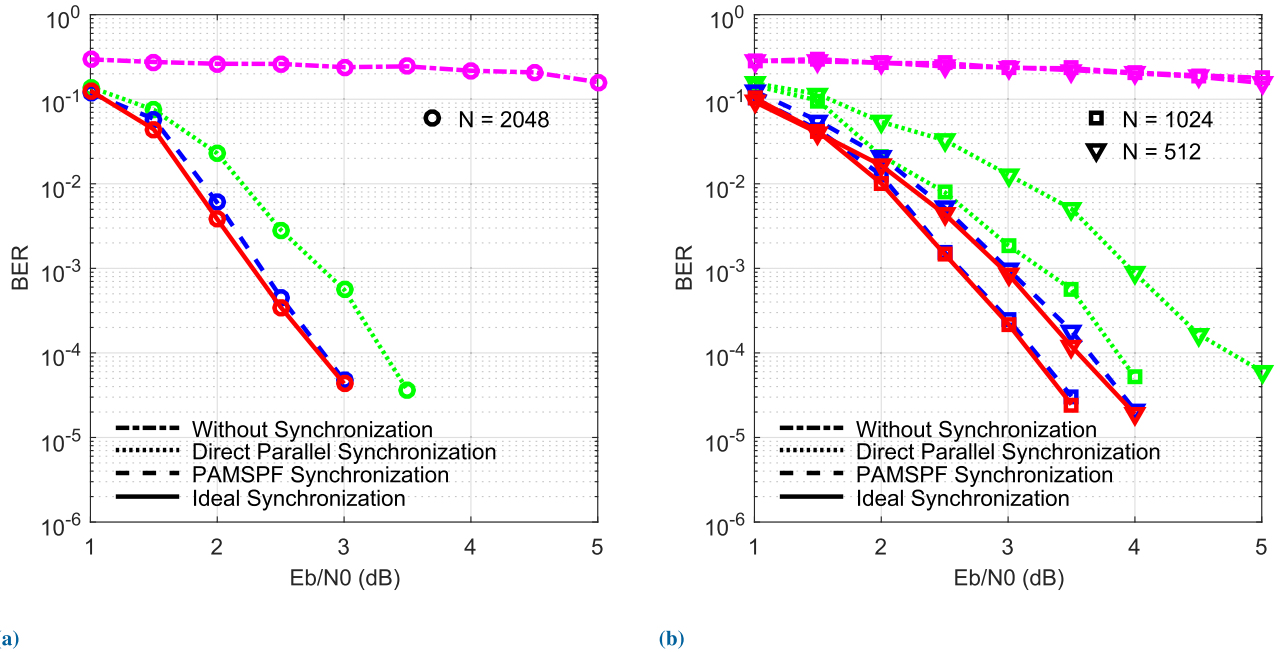
FIGURE 16. BER performance comparison between the PAMSPF synchronization concatenated with PBDC combination algorithm and other synchronization schemes in MCICSC system, where three polar codes C_1, C_2 and C_3 are employed: (a). BER performance comparison while employing C_1; (b). BER performance comparison while employing C_2 and C_3.

Finally, for each data stream, the complexity of CFPO process is mainly imposed by three kinds of calculations: the calculation of ζ_k based on (30), the calculation of updating frequency offset based on (17) and the calculation of updating phase offset based on (18). In more detail, it is clear that for (30) the maximum number of RMDOs will not exceed the length of L_{pos}, which is identical to the codeword length of N. Hence, we may denote the practical number of RMDOs required by calculating (30) as N_ζ, $N_\zeta \leq N$. The number of RMDOs required by calculating (17) is determined by the number of possible $\Delta f T_s$ involved in the whole frequency offset estimation process, which is denoted by N_s. Besides, for each possible value of $\Delta f T_s$, $(8N + N_\zeta + 2)$ RMDOs are required as 4 RMDOs are required for a complex multiplication and 2 RMDOs are required for a squared operation on an absolute value. Hence, the total RMDOs required by (17) can be accounted as $\mathcal{O}(N_s(8N + N_\zeta + 2))$. At last, the phase offset calculation in (18) could be regarded as an angle mapping operation, which may only require a single RMDO.

Based on the above analysis, the complexity of PAMSPF for once carrier synchronization can be rewritten as

$$
\begin{aligned}
\mathcal{C}_{PAMSPF} &\approx I_{outer}\left(\sum_{j=1}^{J}(\mathcal{C}_{BP}(j) + \mathcal{C}_{CFPO}(j) + \mathcal{C}_{PFIM})\right) \\
&\approx \mathcal{O}(JI_{outer}I_{BP}N(N - K)(\bar{d}_c - 2)) \\
&\quad + \mathcal{O}(JI_{outer}(N_s(8N + N_\zeta + 2) + 1)) \\
&\quad + \mathcal{O}(I_{outer}N),
\end{aligned}
\tag{36}
$$

where I_{BP} and N_ζ are related to the practical SNR and would rapidly decrease when the SNR increases.

On the other hand, the RMDO required by the PBDC algorithm mainly imposed by the calculation of the combing coefficients based on (33) and that of the signal summarization based on (32). Thus, its total complexity can be formulated as

$$
\begin{aligned}
\mathcal{C}_{PBDC} &\approx \mathcal{O}(J) + \mathcal{O}(J) \\
&\approx \mathcal{O}(J),
\end{aligned}
\tag{37}
$$

which is proportional to the number of data stream J. It should be further pointed out that the calculation of combining coefficients can share the same information from PAMSPF excluding the calculations involved in (33) and (34). Therefore, the complexity of PBDC algorithm is relative low.

Additionally, in the perspective of hardware implementation, the computing ability required by our PAMSPF can be further relaxed by transforming the parallel structure in Fig. 9 into a serial architecture. After this transformation, the hardware computing ability required by our system becomes similar to that of a system only having a single data stream. It is beneficial for the hardware implementation on resource-limited platforms. In order to realize this transformation, firstly the data streams should be sequentially processed by using a single data stream carrier synchronization architecture. Then, all the associated results are stored and consecutively processed by the PFIM module. As a result, the total hardware computational resources required by the MCICSC system is reduced almost by J times compared with the parallel structure. Furthermore, in practical application, this transformation does not affect diversity combining process. Therefore, in hardware implementation, the serial

and parallel structures can be flexibly adopted according to various demands.

VI. CONCLUSION

In this paper, we realized an intelligent covert satellite communication system for military robot swarms. Firstly, we proposed a novel multi-carrier intelligent covert communication (MCICSC) scheme and provided an advanced method for adapting its configurations to various applications. Then, we designed a polar code-aided carrier synchronization scheme for single data case. We specified its fundamental framework and simulated its performance in low SNR region. Furthermore, we extended the synchronization algorithm of single data stream case to multiple data stream case and applied it to the MCICSC system. As a result, we constructed a polar code-aided multi-stream parallel feedback carrier synchronization architecture. Additionally, we conceived a polar code-based diversity combining scheme, which greatly decreases the complexity of combining process involved in the MCICSC system. Finally, abundant of simulations including RMSE and BER performance are provided, where three kinds of polar codes are tested. These simulation results sufficiently confirmed the advance of our synchronization and combing algorithms proposed for the MCICSC system. Therefore, the proposed MCICSC scheme is expected to play an important role for military robot swarms in the future.

REFERENCES

[1] M. Rubenstein, A. Cornejo, and R. Nagpal, "Programmable self-assembly in a thousand-robot swarm," *Science*, vol. 345, no. 6198, pp. 795–799, Aug. 2014.

[2] E. Martínez-Martín, *Swarm Robotics: From Biology to Robotics*. Rijeka, Croatia: InTech, 2010, ch. 1.

[3] S. Wasilow and J. B. Thorpe, "Artificial intelligence, robotics, ethics, and the military: A canadian perspective," *AI Mag.*, vol. 40, no. 1, pp. 37–48, Apr. 2019.

[4] P. Simon, "Military robotics: Latest trends and spatial grasp solutions," *Int. J. Adv. Res. Artif. Intell.*, Apr. 2015, vol. 4, no. 4, pp. 9–18.

[5] N. Zhao, W. Lu, M. Sheng, Y. Chen, J. Tang, F. R. Yu, and K.-K. Wong, "UAV–assisted emergency networks in disasters," *IEEE Wireless Commun.*, vol. 26, no. 1, pp. 45–51, Feb. 2019.

[6] N. Zhao, X. Pang, Z. Li, Y. Chen, F. Li, Z. Ding, and M.-S. Alouini, "Joint trajectory and precoding optimization for UAV–assisted NOMA networks," *IEEE Trans. Commun.*, vol. 67, no. 5, pp. 3723–3735, May 2019.

[7] F. Cheng, G. Gui, N. Zhao, Y. Chen, J. Tang, and H. Sari, "UAV-relaying-assisted secure transmission with caching," *IEEE Trans. Commun.*, vol. 67, no. 5, pp. 3140–3153, May 2019.

[8] A. K. Maini and V. Agrawal, *Satellite Technology: Principles and Applications*, 3rd ed. Chichester, U.K.: Wiley, 2014, ch. 10.

[9] B. R. Elbert, *Introduction to Satellite Communication*, 3rd ed. Norwood, MA, USA: Artech House, 2008, ch. 2.

[10] W. Zeng, J. Zhang, D. W. K. Ng, B. Ai, and Z. Zhong, "Two–way hybrid terrestrial–satellite relaying systems: Performance analysis and relay selection," *IEEE Trans. Veh. Technol.*, vol. 68, no. 7, pp. 7011–7023, Jul. 2019.

[11] J. Zhang, X. Li, I. S. Ansari, Y. Liu, and K. A. Qaraqe, "Performance analysis of dual–hop DF satellite relaying over k-μ shadowed fading channels," in *Proc. IEEE Wireless Commun. Netw. Conf. (WCNC)*, Mar. 2017, pp. 1–6.

[12] D. Roddy, *Satellite Communications*, 4th ed. New York, NY, USA: McGraw-Hill, 2006, ch. 1.

[13] E. Arikan, "Channel polarization: A method for constructing capacity–achieving codes for symmetric binary–input memoryless channels," *IEEE Trans. Inf. Theory*, vol. 55, no. 7, pp. 3051–3073, Jul. 2009.

[14] L. Kong, J. Bian, S. Zhang, S. Zhao, and Y. Fang, "Polar code design for ultra–high density magnetic recording channels," in *Proc. Asia–Pacific Magn. Recording Conf. (APMRC)*, Nov. 2018, pp. 1–2.

[15] M. S. Mohammadi, I. B. Collings, and Q. Zhang, "Simple hybrid ARQ schemes based on systematic polar codes for IoT applications," *IEEE Commun. Lett.*, vol. 21, no. 5, pp. 975–978, May 2017.

[16] H. Liang, A. Liu, Q. Zhang, and Y. Zhang, "Design of systematic polar coded selective-IR hybrid ARQ transmission for IoT," in *Proc. IEEE/CIC Int. Conf. Commun. China (ICCC)*, Oct. 2017, pp. 1–5.

[17] Z. Che, J. Fang, Z. L. Jiang, J. Li, S. Zhao, Y. Zhong, and Z. Chen, "A physical–layer secure coding scheme for indoor visible light communication based on polar codes," *IEEE Photon. J.*, vol. 10, no. 5, pp. 1–13, Oct. 2018.

[18] K. D. Rao, "Performance analysis of polar codes for 5G short message transmissions," in *Proc. 5th IEEE Uttar Pradesh Section Int. Conf. Electr., Electron. Comput. Eng. (UPCON)*, Nov. 2018, pp. 1–5.

[19] W. K. Abdulwahab and A. A. Kadhim, "Comparative study of channel coding schemes for 5G," in *Proc. Int. Conf. Adv. Sci. Eng. (ICOASE)*, Oct. 2018, pp. 239–243.

[20] O. Iscan, R. Bohnke, and W. Xu, "Probabilistic shaping using 5G new radio polar codes," *IEEE Access*, vol. 7, pp. 22579–22587, 2019.

[21] P. R. Balogun, I. D. Marsland, R. H. Gohary, and H. Yanikomeroglu, "Polar codes for noncoherent MIMO signalling," in *Proc. IEEE Int. Conf. Commun. (ICC)*, May 2016, pp. 1–6.

[22] C. Chen, L. Li, L. Wang, S. Wang, X. Li, and G. K. Karagiannidis, "Noncoherent detection with polar codes," *IEEE Access*, vol. 7, pp. 6362–6372, 2019.

[23] I. Tal and A. Vardy, "List decoding of polar codes," *IEEE Trans. Inf. Theory*, vol. 61, no. 5, pp. 2213–2226, May 2015.

[24] K. Niu and K. Chen, "Stack decoding of polar codes," *Electron. Lett.*, vol. 48, no. 12, p. 695, 2012.

[25] S. Cammerer, M. Ebada, A. Elkelesh, and S. Ten Brink, "Sparse graphs for belief propagation decoding of polar codes," in *Proc. IEEE Int. Symp. Inf. Theory (ISIT)*, Jun. 2018, pp. 1465–1469.

[26] Y. Ren, F. Shu, L. Li, Z. Zhang, X. You, and C. Zhang, "A novel D–metric for blind detection of polar codes," in *Proc. IEEE Int. Workshop Signal Process. Syst. (SiPS)*, Oct. 2018, pp. 106–111.

[27] W. Xu, X. You, C. Zhang, and Y. Berery, "Polar decoding on sparse graphs with deep learning," in *Proc. 52nd Asilomar Conf. Signals, Syst., Comput.*, Oct. 2018, pp. 599–603.

[28] C. Condo, V. Bioglio, and I. Land, "Generalized fast decoding of polar codes," in *Proc. IEEE Global Commun. Conf. (GLOBECOM)*, Dec. 2018, pp. 1–6.

[29] R. Gallager, "Low-density parity-check codes," *IRE Trans. Inf. Theory*, vol. 8, no. 1, pp. 21–28, Jan. 1962.

[30] G. Frèche, M. Bloch, and M. Barret, "Polar codes for covert communications over asynchronous discrete memoryless channels," in *Proc. 51st Annu. Conf. Inf. Sci. Syst. (CISS)*, Mar. 2017, p. 1.

[31] G. Geraci, A. Y. Al-Nahari, J. Yuan, and I. B. Collings, "Linear precoding for broadcast channels with confidential messages under transmit–side channel correlation," *IEEE Commun. Lett.*, vol. 17, no. 6, pp. 1164–1167, Jun. 2013.

[32] L. Ning, L. Kanfeng, L. Wenliang, and D. Zhongliang, "A joint encryption and error correction method used in satellite communications," *China Commun.*, vol. 11, no. 3, pp. 70–79, Mar. 2014.

[33] V. Dasilva and E. Sousa, "Performance of orthogonal CDMA codes for quasi-synchronous communication systems," in *Proc. 2nd IEEE Int. Conf. Universal Pers. Commun.*, vol. 2, Oct. 1993, pp. 995–999.

[34] S. Hara and R. Prasad, "Overview of multicarrier CDMA," *IEEE Commun. Mag.*, vol. 35, no. 12, pp. 126–133, Dec. 1997.

[35] L.-L. Yang and L. Hanzo, "Multicarrier DS-CDMA: A multiple access scheme for ubiquitous broadband wireless communications," *IEEE Commun. Mag.*, vol. 41, no. 10, pp. 116–124, Oct. 2003.

[36] C. Leroux, I. Tal, A. Vardy, and W. J. Gross, "Hardware architectures for successive cancellation decoding of polar codes," in *Proc. IEEE Int. Conf. Acoust., Speech Signal Process. (ICASSP)*, May 2011.

[37] A. Balatsoukas-Stimming, M. Bastani Parizi, and A. Burg, "LLR–based successive cancellation list decoding of polar codes," *IEEE Trans. Signal Process.*, vol. 63, no. 19, pp. 5165–5179, Oct. 2015.

[38] E. Arıkan, "Polar codes: A pipelined implementation," in *Proc. 4th Int. Symp. Broadband Commun.*, Melaka, Malaysia, Jul. 2010.

[39] A. P. Dempster, N. M. Laird, and D. B. Rubin, "Maximum likelihood from incomplete data via the EM algorithm," *J. Roy. Stat. Soc.*, vol. 39, no. 1, pp. 1–22, 1977.

[40] J. Zhang, X. Mu, and L. Hanzo, "Joint channel, carrier-frequency-offset and noise–variance estimation for OFDM systems based on expectation maximization," in *Proc. IEEE 71st Veh. Technol. Conf.*, 2010, pp. 1–5.

[41] E. P. Simon, L. Ros, H. Hijazi, and M. Ghogho, "Joint carrier frequency offset and channel estimation for OFDM systems via the EM algorithm in the presence of very high mobility," *IEEE Trans. Signal Process.*, vol. 60, no. 2, pp. 754–765, Feb. 2012.

[42] C. Herzet, N. Noels, V. Lottici, H. Wymeersch, M. Luise, M. Moeneclaey, and L. Vandendorpe, "Code–aided turbo synchronization," *Proc. IEEE*, vol. 95, no. 6, pp. 1255–1271, Jun. 2007.

[43] J. Yang and B. Zhang, "Artificial intelligence in intelligent tutoring robots: A systematic review and design guidelines," *Appl. Sci.*, vol. 9, no. 10, p. 2078, May 2019.

[44] S. J. Russell and P. Norvig, *Artificial Intelligence 3e: A Modern Approach*. Kuala Lumpur, Malaysia: Pearson Education Limited, 2016.

[45] E. Arikan, "Systematic Polar Coding," *IEEE Commun. Lett.*, vol. 15, no. 8, pp. 860–862, Aug. 2011.

[46] H. Vangala, E. Viterbo, and Y. Hong, "A comparative study of polar code constructions for the AWGN channel," 2015, *arXiv:1501.02473*. [Online]. Available: https://arxiv.org/abs/1501.02473

[47] A. D'Andrea, U. Mengali, and R. Reggiannini, "The modified Cramer–Rao bound and its application to synchronization problems," *IEEE Trans. Commun.*, vol. 42, nos. 2–4, pp. 1391–1399, Feb. 1994.

[48] M. Fitz, "Planar filtered techniques for burst mode carrier synchronization," in *Proc. IEEE Global Telecommun. Conf., Countdown New Millennium. Conf. Rec. (GLOBECOM)*, vol. 1, Dec. 1991, pp. 365–369.

[49] A. Viterbi, "Nonlinear estimation of PSK-modulated carrier phase with application to burst digital transmission," *IEEE Trans. Inf. Theory*, vol. IT-29, no. 4, pp. 543–551, Jul. 1983.

[50] J. Chen, "Reduced complexity decoding algorithms for low-density parity check codes and turbo codes," Ph.D. dissertation, Univ. Hawaii Manoa, Honolulu, HI, USA, 2003.

CHAOFAN CHEN received the B.Eng. degree in communication engineering from the Northwest University for Nationalities, Lanzhou, China, in 2012. He is currently pursuing the Ph.D. degree in communication and information systems with the School of Information and Electronics, Beijing Institute of Technology, Beijing, China.

His research interests include channel coding and its applications, hardware design and implementation of high-speed decoding, non-coherent detection over coded modulation systems, and non-orthogonal multiple access technologies in wireless communications.

SHUAI WANG received the B.Eng. (Hons.) and Ph.D. (Hons.) degrees from Zhengzhou University and Beijing Institute of Technology, China, in 2005 and 2012, respectively, both majoring in communications engineering.

From September 2010 to September 2011, he was a Visiting Ph.D. Student with the School of Electronics and Computer Science, University of Southampton, U.K. He has been with the School of Information Science and Electronics, Beijing Institute of Technology, since July 2012, where he is currently an Associate Professor. He has published more than 20 peer-reviewed articles, mainly in leading IEEE journals or conferences. He also holds 17 patents. His research interests include channel estimation, anti-jamming transmission, synchronization techniques, and beamforming.

Prof. Wang served or is serving as the Principal Investigator for 12 research funds, including two granted by the National Science Foundation of China. He is a recipient of the (Second Class) Scientific and Technical Progress Award granted by the Ministry of Industry and Information Technology of China. He won the award for the "Outstanding Ph.D. Dissertation" granted by the Beijing Municipal Education Commission in 2013 with other 49 co-winners, nominated from all the Ph.D. graduates that received their degree in Beijing that year.
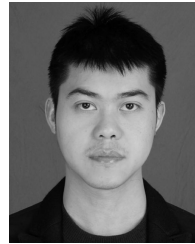
LI LI received the Ph.D. degree from the Southampton Wireless (SW) Group, School of Electronics and Computer Science, University of Southampton, in December 2013.

Upon the completion of his Ph.D. degree, he conducted research as a Senior Research Assistant with the School of Electronics and Computer Science, University of Southampton, from December 2013 to December 2014. In May 2015, he joined the Provincial Key Laboratory of Information Coding and Transmission, Southwest Jiaotong University, Chengdu, China, serving as an Associate Professor. His research interests include channel coding, iterative detection, non-coherent transmission technologies, cooperative communications, network coding, and non-orthogonal multiple access technologies.

SHENG KE received the bachelor's degree in information engineering from the Beijing Institute of Technology (BIT), Beijing, China, in 2013, where he is currently pursuing the Ph.D. degree with the School of Information and Electronics Communication. He has been a Research Assistant with the University of Macau, since May 2018. His research interests are in the fields of wireless communication, physical-layer security, and optimization theory. He was a Reviewer of the IEEE Transactions on Vehicular Technology, the IEEE Transactions on Wireless Communications, and the IEEE International Conference on Communication Systems.
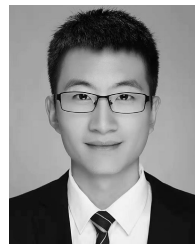
CHANGHONG WANG received the B.Eng. degree in communication engineering from Zhengzhou University, China, in 2013. He is currently pursuing the Ph.D. degree in information and communication engineering with the Beijing Institute of Technology, China. His main research interests include spread spectrum communication, anti-jamming transmission, and digital signal processing. He has contributed to the design and testing of two ASICs that implement the function of spread spectrum transmitter and receiver.

XIANGYUAN BU received the B.Eng. and Ph.D. degrees from the Beijing Institute of Technology (BIT), Beijing, China, in 1987 and 2007, respectively. From 1996 to 1998, he was a Visiting Scholar with the Military Academy of Belarus, Belarus. Since 2002, he has been with the School of Information and Electronics, BIT, where he is currently a Professor. His current research interests include wireless communication, digital signal processing, and channel coding.

● ● ●